Article

Self–Tuning Control Techniques for Wind Turbine and Hydroelectric Plant Systems

Silvio Simani*, Stefano Alvisi and Mauro Venturini

Dipartimento di Ingegneria, Università degli Studi di Ferrara. Via Saragat 1E, Ferrara (FE) 44122, Italy.
{silvio.simani,stefano.alvisi,mauro.ventunini}@unife.it
* Corresponding author. Correspondence: silvio.simani@unife.it; Tel.: +39-0532-97-4844

Abstract: The interest on the use of renewable energy resources is increasing, especially towards wind and hydro powers, which should be efficiently converted into electric energy via suitable technology tools. To this aim, self–tuning control techniques represent viable strategies that can be employed for this purpose, due to the features of these nonlinear dynamic processes working over a wide range of operating conditions, driven by stochastic inputs, excitations and disturbances. Some of the considered methods were already verified on wind turbine systems, and important advantages may thus derive from the appropriate implementation of the same control schemes for hydroelectric plants. This represents the key point of the work, which provides some guidelines on the design and the application of these control strategies to these energy conversion systems. In fact, it seems that investigations related with both wind and hydraulic energies present a reduced number of common aspects, thus leading to little exchange and share of possible common points. This consideration is particularly valid with reference to the more established wind area when compared to hydroelectric systems. In this way, this work recalls the models of wind turbine and hydroelectric system, and investigates the application of different control solutions. The scope is to analyse common points in the control objectives and the achievable results from the application of different solutions. Another important point of this investigation regards the analysis of the exploited benchmark models, their control objectives, and the development of the control solutions. The working conditions of these energy conversion systems will be also taken into account in order to highlight the reliability and robustness characteristics of the developed control strategies, especially interesting for remote and relatively inaccessible location of many installations.

Keywords: Wind turbine system; hydroelectric plant simulator; model–based control; data–driven approach; self–tuning control; robustness and reliability

1. Introduction

The trend to reduce the use of fossil fuels, motivated by the need to meet greenhouse gas emission limits, has driven much interest on renewable energy resources, in order also to cover global energy requirements. Wind turbine systems, which now represent a mature technology, have had much more development with respect to other energy conversion systems, *e.g.* for biomass, solar, and hydropower [1,2]. In particular, hydroelectric plants present interesting energy conversion potentials, with commonalities and contrast with respect to wind turbine installations [3–5].

One common aspect regarding the design of the renewable energy conversion system concerns the optimality and the efficiency of its converter. However, as wind and hydraulic resources are free, the key point is represented by the minimisation of the cost per kWh, also considering the lifetime of the deployments. Moreover, when the capital, operational and commissioning/decommissioning

costs are fixed, the value of the energy sold (*i.e.* the energy receipts) has to be maximised. This represents a fundamental economic objective, which should be carefully taken into account also by the design of the control system. Indeed, the design of the device should follow a top–down development. However, as first step, physicists propose the energy conversion system design, whilst system engineers investigate the control problem in a subsequent phase, in cooperation with the discipline–specific experts. This approach is common in most industrial applications of control, but it can lead to non–optimal solutions.

It is worth noting that preliminary works highlighted interactions between the renewable energy conversion system design and the strategies exploited to control them, see for example, [6]. Moreover, by taking into account that the cost of control system technology (*i.e.* sensors, actuators, computer, software) is relatively lower than the one of the renewable energy converter [7], the control system should aim at increasing the energy conversion capacity of the given plant. However, this strategy neglects the control system capability and the engineering expertise required for the development of a suitable control technique. As an example, model–based control design schemes need for a high–fidelity mathematical model of the process to be controlled, which could have required a significant number of man–hours to achieve it. On the other hand, increasing efforts are made for integrating the control technology efficiency and its performances (both technical and economic), with the reliability and safety features of the controlled system, as discussed *e.g.* in [8]. By considering these aspects in particular for wind turbine installations and hydroelectric plants, this paper will analyse different model–based and data–driven control techniques that are more effective than their baseline governors.

Note also that several economic aspects have to be considered when designing control schemes for renewable energy conversion devices. One important point is that wind turbine processes and hydroelectric plants can be installed in relatively remote and inaccessible areas, with obvious implications for operation requirements and maintenance services. To this aim, the control technique must be designed to be robust and reliable, thus motivating the need for fault–tolerant control features (also known as 'sustainable') [9].

It is quite established that the mathematical descriptions of both wind turbine processes and hydroelectric plants are represented by nonlinear dynamic processes working over a wide range of operating conditions and excitations. These systems are also required to operate under specific physical constraints, such as displacements, velocities, accelerations, torques and forces. Therefore, these systems can operate effectively with economically attractive and high operational lifetimes only if their working conditions are carefully fulfilled. With these issues in mind, the paper recalls the mathematical description of a wind turbine system and a hydroelectric plant, by using a wind turbine benchmark and a hydroelectric simulator, respectively. The former process was proposed for the purpose of an international competition started in 2009 and described in detail [10], whilst the latter system was developed by the same authors, and presented for the first time in [11]. On the other hand, this work analyses different control strategies for both wind turbines and hydroelectric systems that can show common and different aspects. Moreover, in general, when considering on–grid plants, the control system has to consider also the regulation of the voltage and frequency, which will not be addressed in this work.

After these remarks, by means of the analysis of the proposed modelling and control topics, the work will sketch common and different aspects of wind turbines and hydraulic systems, which will be exploited for the design of the control technique. On one hand, hydroelectric power plants result to be more established and even more common than wind turbine processes, but the control aspects for the latter systems have been examined more in depth in the last decades.

With reference to wind turbine systems, it can be observed that modern installations exploit control techniques and technologies in order to obtain the needed goals and performance achievements. These plants can implement their regulation via 'passive' control methods, such as the plants with fixed–pitch, and stall control machines. The blades of these systems are deployed in

order to limit their power via the blade stall, when the wind speed exceeds its rated value. These systems do not need any pitch control mechanism, as addressed *e.g.* in [12]. Moreover, these plants implement a simple rotational speed control, thus avoiding the inaccuracy problems derived from the measurement of the wind speed [10]. On the other hand, wind turbine rotors using adjustable pitch systems are often exploited in constant–speed installations, in order to overcome the limitations due to the simple blade stall and to improve the converted power [13]. Therefore, in order to increase the generated power below the rated wind speed, the wind turbine has to modify its rotational speed with the wind velocity. To this aim, the regulation of the blade pitch is exploited only above the rated wind speed to control the generated power [14]. Large wind turbines can implement another control technique modifying the yaw angle, which is used to orient the rotor towards the wind direction. In this way, a yaw error signal is generated from a nacelle–mounted wind direction sensor, which is thus exploited to control the yaw motor when the error exceeds certain limits, as described *e.g.* in [15].

It is worth noting that a limited number of works have addressed the development of self–tuning control techniques for hydroelectric plants, as shown *e.g.* in [16]. In fact, a high–fidelity mathematical description of these processes can be difficult to be achieved in practice. However, some contributions reported the analytical formulation of hydroelectric plants, together with the design of their control strategies. Note that these papers took into account the elastic water effects, even if the nonlinear dynamics are linearised around an operating condition. Moreover, other contributions, see *e.g.* [17], proposed different mathematical models together with the strategies exploited to control these systems. In the same way, linear and nonlinear dynamic processes with different water column effects and regulation strategies are also proposed. For example, [18] considered advanced control techniques for hydraulic processes.

In the light of these considerations, the paper also proposes to analyse those control aspects that might be similar between wind turbine and hydroelectric systems, with the aim of exploiting some solutions, developed in the wind turbine domain, and to apply them within the other concerning hydroplants. This approach could be used to stimulate novel research topics and the development of innovative techniques in a multidisciplinary control community, and the most important achievements will be summarised in this paper. In particular, suitable analytical models of these energy conversion plants should be able to provide the overall dynamic behaviour of the monitored processes, thus leading important impacts on the development of the control techniques. Moreover, the work introduces some kind of common rules for tuning the different controllers, for both wind turbine and hydroelectric plants. Therefore, the paper shows that the parameters of these controllers are obtained by exploiting the same tuning strategies. This represents one of the key contributions of the study.

Note that some previous studies by the same authors addressed several topics presented in this paper. For example, the work [19] considered control techniques when applied only to the hydroelectric simulator, which were not compared to the wind turbine benchmark. On the other hand, the paper [20] performed an overview of the main modelling and control strategies, in particular for wind turbines and wave energy devices: the hydroelectric plant benchmark and the simulations of the proposed control techniques were not addressed. Moreover, the earlier work [11] presented the hydroelectric simulator, but considered only the design of standard PID regulator for the optimisation of its time response. Finally, the paper [21] developed a fault tolerant control methodology by means of differential algebraic tools using a purely nonlinear mathematical formulation of the wind turbine system. Other more recent control techniques applied to wind turbine systems were investigated *e.g.* in [22,23].

It is worth highlighting the main contribution of the paper, which aims at providing some guidelines on the design and the application of self–tuning control strategies to two energy conversion systems. Some of these techniques were already verified on wind turbine systems, and important advantages may thus derive from the appropriate implementation of the same control methods for hydroelectric plants. In fact, it seems that investigations related with both wind and

 doi:10.20944/preprints201810.0572.v1

hydraulic energies present a reduced number of common aspects, thus leading to little exchange and share of possible common points. This consideration is particularly valid with reference to the more established wind area when compared to hydroelectric systems. In this way, the paper summarises also the most common models used for describing wind turbine and hydroelectric systems. Moreover, it analyses the application of the different control solutions to these energy conversion systems. The aim is thus to exploit common points in the control objectives and the achievable results from the application of different solutions. Another important point of this paper concerns the discussion of the exploited benchmark models, their control objectives, and the development of the control solutions. The working conditions of these energy conversion systems will be also taken into account in order to highlight the reliability and robustness characteristics of the developed control strategies.

Finally, the paper has the following structure. Section 2 provides the brief presentation of the benchmark and simulation models used for describing the accurate behaviour of the dynamic processes. Section 3 discusses the specific requirements of the control systems exploited to control these energy conversion plants. Section 3.1 summarises the design of the proposed model–based and data–driven control techniques, taking into account the control objectives and the available tools. In Section 4, these self–tuning control strategies are implemented and compared, with respect to the achievable reliability and robustness features. Section 5 ends the paper summarising the main achievements of the paper, and drawing some concluding remarks.

2. Simulator Models and Reference Governors

This section recalls the simulators used for describing the dynamic behaviour of the wind turbine and the hydroelectric processes considered in this paper. Moreover, the baseline control schemes developed for the regulation of the wind turbine benchmark are also summarised in Section 2.1. On the other hand, the hydroelectric simulator, together with its reference governor, is recalled in Section 2.2.

2.1. Wind Turbine System Benchmark

Industrial wind turbine installations are normally equipped with large rotors, flexible blades and light load–carrying structures, which work in uncertain environments, often placed in remote and inaccessible places [24]. These topics have motivated the use of high–fidelity simulators and the development of proper control solutions, which could cope with these challenging technologies. These control strategies should thus be able to obtain prescribed performances, such as decreasing the produced energy cost, increasing the energy conversion effectiveness, reducing downtimes, and maximising the installation lifetime [8]. To this aim, the control scheme should also reduce the structural loads, torques and induced vibrations, thus increasing the lifetime of the overall installation [25]. These challenging topics will not be considered in this work, which represent recent research topics in the frameworks of both wind turbine systems and hydroelectric power plants. However, this paper will consider the design and the application of self–tuning control techniques that are able to optimise the tracking of a given reference. This reference or set–point signal guarantees the maximisation of the energy production [6].

In particular regarding wind turbines, even if they are designed in both horizontal– and vertical–axis solutions, this work focuses on a horizontal–axis device, which nowadays represents the most common type of installation for large–scale deployments. Moreover, the three–bladed horizontal axis wind turbine model reported in this work follows the principle that the wind power activates the wind turbine blades, thus producing the rotation of the low speed rotor shaft. In order to increase its rotational speed generally required by the generator, a gear–box with a drive–train is included in the system. A more detailed picture of this benchmark that was proposed for an international competition but with different purposes is given *e.g.* in [10]. The schematic diagram of this benchmark that helps to recall its main variables and function blocks developed in the Simulink

Preprints (www.preprints.org) | NOT PEER-REVIEWED | Posted: 24 October 2018 doi:10.20944/preprints201810.0572.v1

environment is depicted in Fig. 1 (b), while the diagram showing its working principles is sketched in Fig. 1 (a).

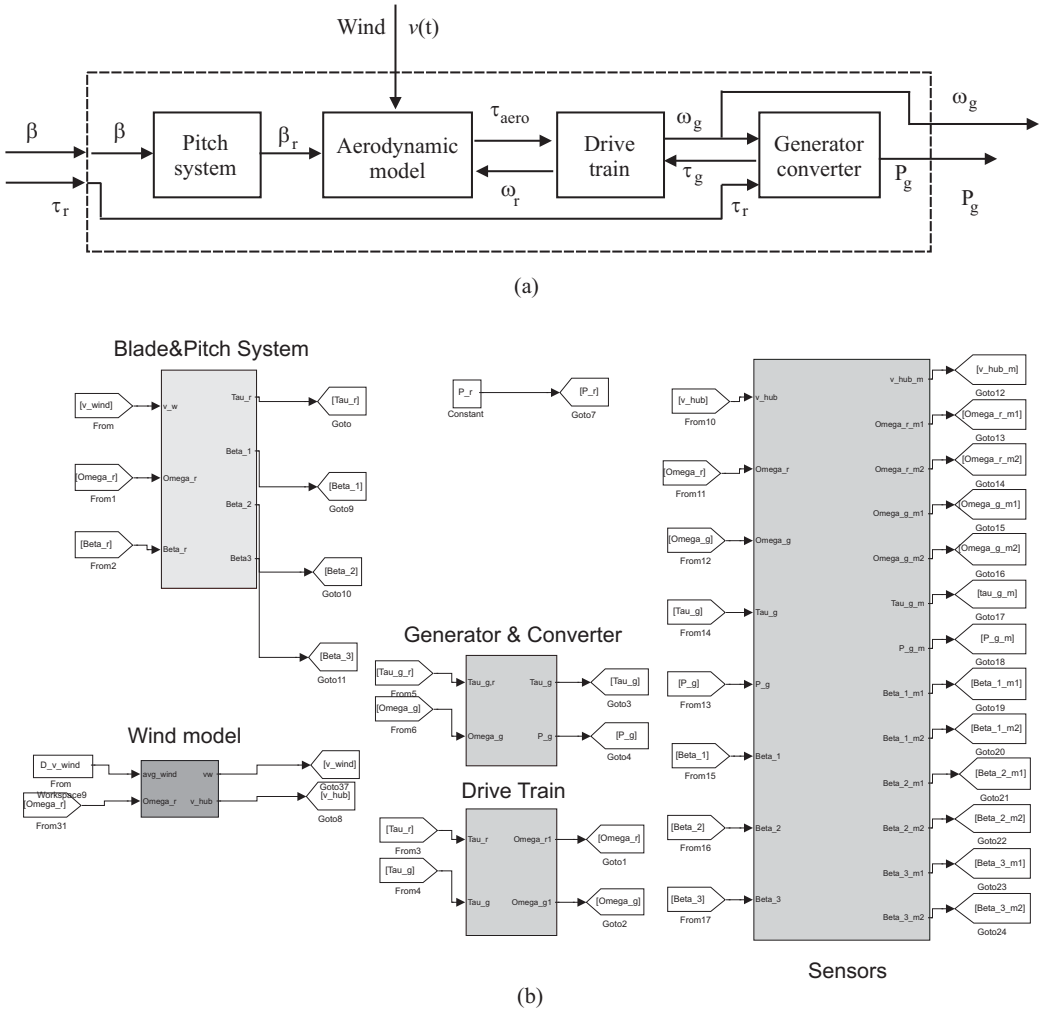

Figure 1. (a)Block diagram of the wind turbine plant, and (b) its benchmark with function blocks.

The wind turbine simulator presents 2 controlled outputs, *i.e.* the generator rotational speed $\omega_g(t)$ and its generated power $P_g(t)$. The wind turbine model is controlled by means of two actuated inputs, *i.e.* the generator torque $\tau_g(t)$ and the blade pitch angle $\beta(t)$. The latter signal controls the blade actuators, which can be implemented by hydraulic or electric drives. The benchmark considered in this work includes a hydraulic circuit actuating the wind turbine blades [10].

Several other measurements are acquired from the wind turbine benchmark: the signal $\omega_r(t)$ represents the rotor speed and $\tau_r(t)$ is the reference torque. Moreover, aerodynamic torque signal $\tau_{aero}(t)$ is computed from the wind speed $v(t)$, which is usually available with limited accuracy. In fact, the wind field is not uniform around the wind turbine rotor plane, especially for large rotor systems. Moreover, anemometers measuring this variable are mounted behind the rotor on the nacelle. Therefore, the wind speed measurement $v(t)$ is affected by the interference between the blades and the nacelle, as well as the turbulence around the rotor plane. Furthermore, when these instantaneous wind fields are considered across the rotor plane, the wind variable $v(t)$ may change in space and time, and it is especially true in large rotor installations. The alteration of the wind speed measurement $v(t)$ with respect to its nominal value around the rotor plane represents an uncertainty in the wind turbine model and a disturbance term in control design. On the other hand,

Preprints (www.preprints.org) | NOT PEER-REVIEWED | Posted: 24 October 2018 doi:10.20944/preprints201810.0572.v1

the aerodynamic torque depends on another factor, C_p, representing the power coefficient, as shown by Eq. (1):

$$\tau_{aero}(t) = \frac{\rho\, A\, C_p\,(\beta(t),\, \lambda(t))\; v^3(t)}{2\,\omega_r(t)} \tag{1}$$

ρ being air density, A the area swept by the turbine blades during their rotation, whilst $\lambda(t)$ represents an important variable, *i.e.* the tip–speed ratio of the blade, which is given by the relation of Eq. (2):

$$\lambda(t) = \frac{\omega_r(t)\, R}{v(t)} \tag{2}$$

where R is the rotor radius. The nonlinear static function $C_p(\cdot)$ represents the power coefficient, which is usually modelled via a two–dimensional map (or look–up table), as highlighted *e.g.* in [10]. The relation of Eq. (1) is exploited to derive the variable $\tau_{aero}(t)$ assuming an uniform measurement $v(t)$, together with the acquired signals $\beta(t)$ and $\omega_r(t)$. As remarked above, the uncertainty affecting the wind speed $v(t)$ leads to an error in the derivation of the variable $\tau_{aero}(t)$ [10]. Moreover, the overall nonlinear behaviour represented by the relations of Eqs. (1) and (2) is reported in Figure 2. The picture is sketched for different values of the variable $\lambda(t)$, depending on the signals $v(t)$ and $\beta(t)$.

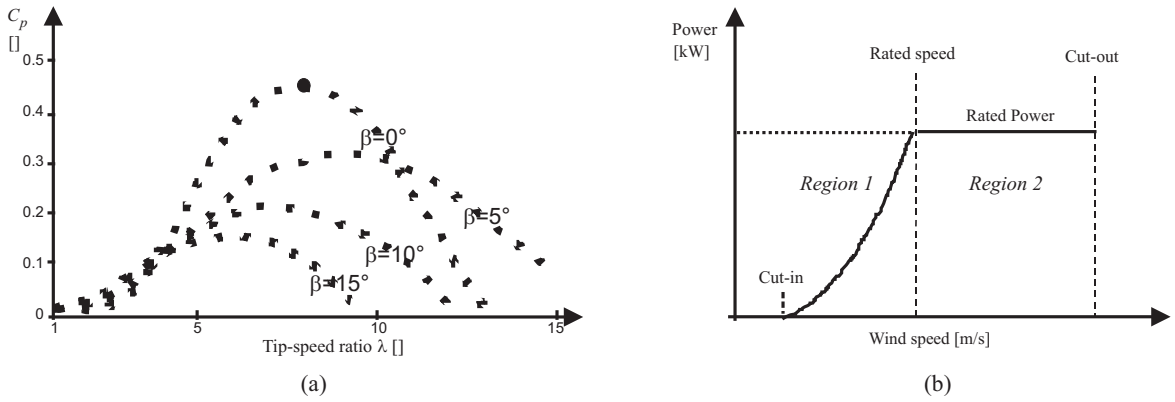

Figure 2. Examples of power coefficient function (a) and power curve (b).

It is worth noting that diagram in Figure 2 (b) represents the power curve highlighting the working conditions of the wind turbine system, also known as partial load (region 1) and full load (region 2) operating situations of the plant [10].

The wind turbine benchmark considered in this work includes a simple two–body linear model of the third order that is exploited to describe the dynamic behaviour of the drive–train. It implements also a simple first–order linear dynamic model of the electric generator and a second order dynamic description of the pitching system, as addressed in more detail in [10]. The overall continuous–time representation of the wind turbine benchmark is represented by the general model in form of Eq. (3):

$$\begin{cases} \dot{x}(t) &= f_c\,(x(t), u(t)) \\ y(t) &= x(t) \end{cases} \tag{3}$$

with $u(t) = [\tau_r(t)\, \beta(t)]^T$ and $y(t) = [\omega_g(t)\, P_g(t)]^T$ are the manipulated input signals and the controlled output measurements, respectively. $f_c\,(\cdot)$ is described by means of a continuous–time nonlinear function that will be exploited for representing the complete dynamic behaviour of the controlled process. Moreover, since this paper will analyse several data–driven control approaches, this system will be used to acquire a number of N sampled data sequences $u(k)$ and $y(k)$, with

Preprints (www.preprints.org) | NOT PEER-REVIEWED | Posted: 24 October 2018 doi:10.20944/preprints201810.0572.v1

$k = 1, 2, \ldots N$. Furthermore, the variables and parameters of the wind turbine benchmark submodels (see *e.g.* Fig. 1), the static function $C_p(\beta, \lambda)$, as well as the errors and uncertain effects affecting the input–output measurements were implemented in the simulation code in order to provide a high–fidelity wind turbine plant simulator, as highlighted in [10]. In particular, the input and output measurements, which are acquired from the wind turbine benchmark, are assumed to be actuated and measured by realistic devices introducing additive Gaussian noise processes with zero mean and standard deviation values summarised in Table 1 [24].

Table 1. Gaussian noise standard deviations of the wind turbine variables.

Variable	$v(t)$	ω_r	ω_g	τ_g	P_g	β
Std. Dev. Value	0.5 m/s	0.025 rad/s	0.05 rad/s	90 Nm	10^3 W	0.2 deg

As already highlighted by Fig. 2 (b), the wind turbine control task depends on its working conditions [10]. However, as the wind turbine benchmark recalled in this work operates in nominal conditions, only 2 regions are analysed, as remarked above. In particular, when operating in the working region 1, the turbine is regulated to achieve the optimal power production (below the rated wind speed). On one hand, with reference again to Fig. 2 (b), this is obtained with the blade pitch angle β fixed to 0 degrees. On the other hand, the tip–speed ratio λ of Eq. (2) is settled at its optimal value K_{opt}. These conditions are obtained according to the peak value of the power coefficient function of the wind turbine, already represented in Figure 2 (a). In this optimal working condition, the reference torque equals the converter one, *i.e.* $\tau_g = \tau_r$, as described by the relation of Eq. (4):

$$\tau_r = K_{opt}\,\omega_r^2 \tag{4}$$

In this situation, the optimal tracking of the power reference is obtained, as soon as the wind speed $v(t)$ increases, and the working condition moves to to the control region 2. The control task aims also at tracking the power reference P_r, which is achieved by modifying β, while C_p is decreasing. The advanced control strategies considered in this work tries to maintain the generator speed ω_g at its nominal value ω_{nom} by changing both β and τ_g.

Therefore, the control system operating in region 2 exploits the relations in the form of Eqs. (5) when implemented as difference equations [10]:

$$\begin{cases} \beta(k) &= \beta(k-1) + k_p\, e(k) + \left(k_i\, T_s - k_p\right)\, e(k-1) \\ e(k) &= \omega_g(k) - \omega_{nom} \end{cases} \tag{5}$$

where $k = 1, 2, \ldots, N$ corresponds to the sample indices, and the variable ω_{nom} is the given reference generator speed, depending on the wind turbine plant. For the case of the wind turbine system considered in this work, $P_r = 4.8MW$ is the rated power, and $\omega_{nom} = 162.5rad/s$. The standard PI governor parameters used for the speed control task were settled to $k_i = 0.5$ and $k_p = 3$, with sampling time $T_s = 0.01$ s [10].

Concerning the regulation of the second input τ_g, a further standard PI governor is implemented in the wind turbine benchmark, similarly to the one of Eq. (5), which is described again in its discrete–time formulation of Eqs. (6):

$$\begin{cases} \tau_r(k) &= \tau_r(k-1) + k_p\, e(k) + \left(k_i\, T_s - k_p\right)\, e(k-1) \\ e(k) &= P_g(k) - P_r \end{cases} \tag{6}$$

This standard PI regulator exploited in the benchmark for the power control task has its parameters settled to $k_i = 0.014$ and $k_p = 447 \times 10^{-6}$, as proposed in [10]. Note that the discrete–time regulators

Preprints (www.preprints.org) | NOT PEER-REVIEWED | Posted: 24 October 2018 doi:10.20944/preprints201810.0572.v1

of Eqs. (5) and (6) implemented in the wind turbine benchmark and recalled in this study were simulated with a frequency of 100 Hz, *i.e.* with a sampling interval of $T_s = 0.01$ s.

Finally, Section 4 will consider the performances of these baseline controllers summarised by the overall laws of Eqs. (4), (5) and (6) proposed in [10] in comparison with the self–tuning control techniques recalled in Section 3. These methodologies will be applied to both the wind turbine and the hydroelectric systems, thus highlighting common and different aspects of these solutions with respect to their working conditions.

2.2. Hydroelectric Plant Simulator

It is well–established that hydroelectric systems transform hydraulic renewable source into useful energies, mostly electric but also mechanical one. However, as for wind turbines, they must operate according to different load situations. In general, hydroelectric plants must operate despite of possible variations in the hydropower flow, and in particular in both planned or nominal conditions and accidental or unplanned situations. Moreover, routine operations such as start–up, shutdown, load rejection and acceptance may induce important hydraulic transients, possible leading to dangerous high pressure and sub–pressure variations and oscillations in the hydraulic system. These situations must be analysed in order to avoid possible mechanical malfunctions and failures. The same simulation codes already exploited for the development of the wind turbine benchmark described in Section 2.1, *i.e.* Matlab and Simulink, are the tools exploited for modelling, simulating, and analysing the behaviour of hydroelectric plants that exhibit important nonlinear dynamics, as addressed earlier *e.g.* in [26]. More recently, hydropower systems including Pumps as Turbines (PATs) have been considered by the same authors, since they present challenging aspects in connection with the control design problem, mainly when implemented for water distribution network and pipeline applications [27]. In fact, general hydropower plants include special control techniques to guarantee stable and safe working conditions. Therefore, the same self–tuning control methodologies already developed for wind turbine systems, as summarised in Section 3, will be considered for the hydroelectric process described in this paper. Note that, due to the design features of the considered self–tuning control solutions, they have shown to work properly also when applied to hydroelectric plants.

With reference to the hydroelectric system, which is recalled in this work for analysis and comparison purposes, consists of a high water head and a long penstock. It includes also upstream and downstream surge tanks, where a Francis hydraulic turbine is included [28]. This hydroelectric simulator considered in earlier studies by the same authors, see *e.g.* [11], served to analyse the transient behaviour of the process with different control schemes. More recent contributions by the same authors reconsidered the same simulator but for the development of data–driven and model–based fault diagnosis and fault tolerant control solutions [29]

The scheme of this hydroelectric simulator including two surge tanks and the Francis hydraulic turbine considered in this work is recalled in Fig. 3 [11]. As already remarked, but recalled here for the readers' convenience, the hydroelectric simulator includes a reservoir with water level H_R, an upstream water tunnel with cross-section area A_1 and length L_1, an upstream surge tank with cross–section area A_2 and water level H_2 of appropriate dimensions. A downstream surge tank with cross–section area A_4 and water level H_4 follows, ending with a downstream tail water tunnel of cross–section area A_5 and length L_5. Moreover, between the Francis hydraulic turbine and the two surge tanks, there is a the penstock with cross–section area A_3 and length L_3. Finally, the right far side of Fig. 3 (a) highlights a tail water lake with level H_T. The levels H_R and H_T of the reservoir and the lake water, respectively, are assumed to be constants. Fig. 3 (b) depicts also the scheme of the pure hydraulic system, and Fig. 3 (c) shows the complete hydroelectric plant simulator.

The mathematical description of the pure hydraulic system, depicted in Fig. 3 (b), which does not include the Francis hydraulic turbine, was proposed earlier in [26] and later in [30]. This model was modified by the authors and presented for the first time in [11]. By considering a pressure water

Preprints (www.preprints.org) | NOT PEER-REVIEWED | Posted: 24 October 2018 doi:10.20944/preprints201810.0572.v1

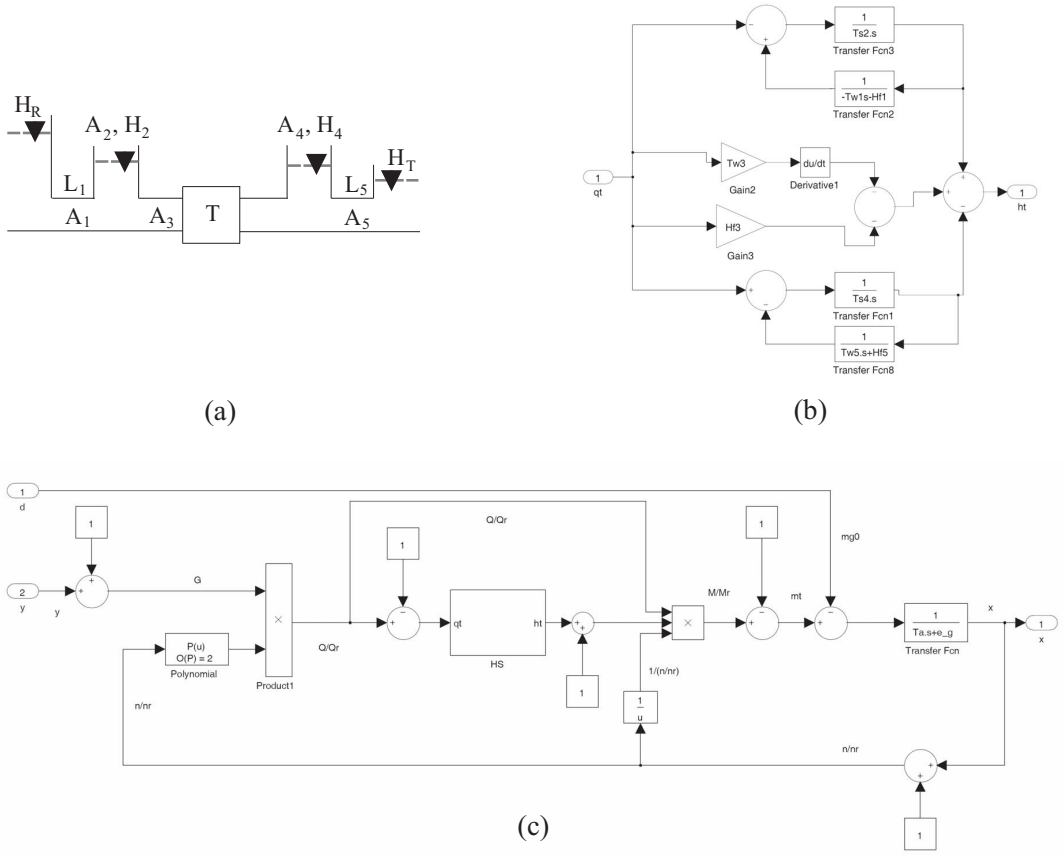

Figure 3. Overall scheme of the hydroelectric process, (b) the hydraulic system, and (c) its complete simulator.

supply system, as addressed in [31], the expressions of the Newton's second law for a fluid element inside a pipe and the conservation mass law for a control volume can be derived, which take into account the water compressibility and the pipe elasticity. If the penstock is assumed to be relatively short, the water and pipelines are considered incompressible. In this conditions, only the inelastic water hammer effect needs to be considered. Therefore, the simplified and general relation of the penstock has the form of Eq. (7):

$$\frac{h}{q} = -T_w\, s - H_f \tag{7}$$

as suggested in [31].

Moreover, Eq. (7) represents the transfer function between the flow rate deviation and the water pressure deviation valid for a simple penstock. The variable h represents the water pressure relative deviation, whilst q is the flow rate relative deviation. The term H_f represents the hydraulic loss, with s the Laplace operator, and T_w the water inertia time expressed by the relation of Eq. (8):

$$T_w = \frac{L\, Q_r}{g\, A\, H_r} \tag{8}$$

Note that the time variable T_w of the water inertia described by the relation of Eq. (8) is a function of the hydraulic variable, such as the penstock length L, the rated flow rate Q_r, the gravity acceleration g, the cross–section area A, and the rated water pressure H_r. The classic plant represented in Fig. 3 (b) can be separated into 3 subsystems, and namely the upstream water tunnel, the penstock, and the downstream tail water tunnel. The transfer functions between the flow rate deviation and water

Preprints (www.preprints.org) | NOT PEER-REVIEWED | Posted: 24 October 2018 doi:10.20944/preprints201810.0572.v1

pressure deviation transfer functions of the three subsystems are summarised below, by following the approach proposed in [31]. In this hydraulic system, the upstream water tunnel is connected with the reservoir and together with the upstream surge tank. Moreover, taking into account that the upstream water tunnel inlet coincides with the reservoir, and due to the constant value of the inlet water pressure deviation during hydraulic transients, the transfer function between the flow rate and the water pressure deviations of the upstream water tunnel outlet has the form of Eq. (9):

$$\frac{h_1}{q_1} = -T_{w_1}\, s - H_{f_1} \tag{9}$$

On the other hand, the downstream tail water tunnel connects the downstream surge tank with the tail water lake. The downstream tail water tunnel outlet is assumed to coincide with the tailwater lake, with constant outlet water pressure deviation. In this way, the transfer function between the flow rate and the water pressure deviations of the downstream tail water tunnel inlet is represented in the form of Eq. (10):

$$\frac{h_5}{q_5} = -T_{w_5}\, s - H_{f_5} \tag{10}$$

Usually, the draft tube water inertia is considered within the penstock. Therefore, the transfer function between the flow rate and the water pressure deviations within the penstock are expressed by the relation of Eq. (11):

$$h_t = h_2 - h_4 + h_3 \tag{11}$$

with:

$$\frac{h_3}{q_3} = -T_{w_3}\, s - H_{f_3} \tag{12}$$

The relations describing the surge tanks are formulated from the flow continuity at the two junctions, by neglecting the hydraulic losses at surge tank orifices, and represented via the relations of Eqs. (13):

$$\begin{cases} \frac{A_2\, H_r}{Q_r}\, \frac{dh_2}{dt} &= q_2 = q_1 - q_3 \\ \frac{A_4\, H_r}{Q_r}\, \frac{dh_4}{dt} &= q_4 = q_3 - q_5 \end{cases} \tag{13}$$

In this situation, the surge tank filling time has the form of Eq. (14):

$$T_s = \frac{A\, H_r}{Q_r} \tag{14}$$

Once the description of the hydraulic system of Fig. 3 (b) was developed as proposed in [30], the authors included the Francis turbine. Its mathematical model and performance curves summarised in this work were obtained in order to describe the dynamic behaviour of a realistic hydroelectric process, as addressed in [32]. To this aim, the values of the most important variables the hydraulic system and the Francis hydraulic turbine, which represent the overall hydroelectric process simulator working at rated conditions are summarised in Table 2:

After these considerations, in the following the procedure for computing the non–dimensional performance curves of the hydraulic turbine considered in this work is briefly recalled. In particular, the non–dimensional water flow rate Q/Q_r is expressed as a function of the non–dimensional rotational speed n/n_r, and represented by the second order polynomial of Eq. (15):

$$\frac{Q}{Q_r} = G\left[a_1 \left(\frac{n}{n_r}\right)^2 + b_1 \left(\frac{n}{n_r}\right) + c_1\right] = f_1\,(n, G) \tag{15}$$

Moreover, the relation of Eq. (15) includes the wicked gate opening, described by the non–dimensional parameter G, varying from 0 to 100%. In particular, Fig. 4 represents the curve

Preprints (www.preprints.org) | NOT PEER-REVIEWED | Posted: 24 October 2018 doi:10.20944/preprints201810.0572.v1

Table 2. Values of the main parameters of the hydroelectric plant simulator.

Variable	Description	Value
H_r	Reservoir water level	400 m
Q_r	Water flow rate	36.13 m^3/s
P_r	Hydraulic turbine power	127.6 MW
n_r	Turbine rated rotational speed	500 rpm
η_r	Efficiency rated value	0.90
M_r	Turbine–rated torque	2437 kNm

derived for $G = 100\%$, *i.e.* fully open wicked gate. Moreover, the curve at $\eta = 0\%$ is also depicted, thus defining the operating conditions of the Francis hydraulic turbine. Furthermore, the same polynomial curve of Eq. (15) allows the computation of the water flow rate Q as a function of the hydraulic turbine rotational speed n and its wicked gate opening G for all working conditions.

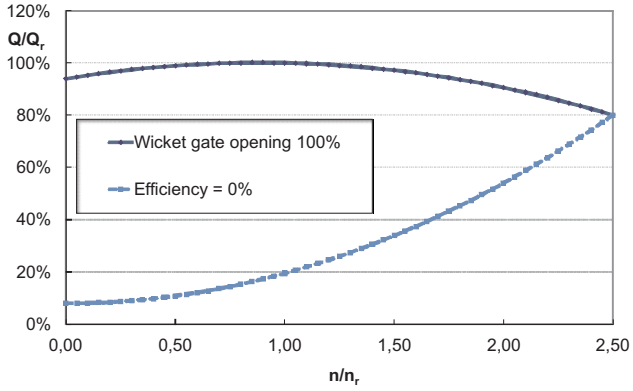

Figure 4. Representation of the non–dimensional water flow rate Q/Q_r with respect to the non–dimensional rotational speed n/n_r.

The hydroelectric simulator assumes that the turbine efficiency is constant and equal to its rated value η_r, *i.e.* 0.9, as reported in Table 2. Note that the hydroelectric simulator does not include possible efficiency variation with the electric load, even if the turbine efficiency η_r could be a function of the non–dimensional rotational speed n/n_r.

On the other hand, the non–dimensional turbine torque M results a function of the water flow rate Q, the water level H and the rotational speed n, as highlighted by the relation of Eq. (16):

$$\frac{M}{M_r} = \frac{\frac{Q}{Q_r}\frac{H}{H_r}}{\frac{n}{n_r}} = f_2\left(Q, n, G\right) \tag{16}$$

Moreover, the combination of the relations of Eqs. (15) and (16) highlights that the turbine torque M is a function of the water flow rate Q, the rotational speed n and wicked gate opening G.

Preprints (www.preprints.org) | NOT PEER-REVIEWED | Posted: 24 October 2018 doi:10.20944/preprints201810.0572.v1

Finally, the overall model of the hydroelectric simulator is described by the relations of Eqs. (17) – (20), which express the non–dimensional variables with respect to their relative deviations:

$$\frac{Q}{Q_r} = 1 + q_t \tag{17}$$

$$\frac{H}{H_r} = 1 + h_t \tag{18}$$

$$\frac{n}{n_r} = 1 + x \tag{19}$$

$$G = 1 + y \tag{20}$$

with q_t is the turbine flow rate relative deviation, h_t the turbine water pressure relative deviation, x the turbine speed relative deviation, and y the wicket gate servomotor stroke relative deviation. Moreover, the relation of Eq. (20) allows only negative values of y.

On the other hand, when the generator unit and its network are considered, and in particular the generator unit is connected only to an isolated load, the load characteristic of the the generator unit are described by the dynamic model of Eq. (21):

$$\frac{x}{m_t - m_{g0}} = \frac{1}{T_a\, s + e_g} \tag{21}$$

with m_{g0} being the load torque, T_a representing the generator unit mechanical time, whilst the parameter e_g is the load self–regulation factor. The variables and parameters of the hydroelectric model were selected according to the work [30] in order to represent a realistic hydroelectric plant simulator. Moreover, as for the wind turbine benchmark, the signals that can be acquired from the actuator and sensors of the hydroelectric plant are modelled as the sum of the actual variables and stochastic noises, as proposed in [33].

With reference to the control strategies for classic hydroelectric plants, standard PID regulators are used to compensate the hydraulic turbine speed. Therefore, the actuated signal u is computed as sum of the proportional, integral, and differential terms of the error x in Eq. (19), expressed in the form of Eq. (22):

$$u = x \left(K_p + \frac{K_i}{s} + \frac{K_d\, s}{1 + T_n\, s} \right) \tag{22}$$

with K_p being the proportional gain, K_i the integral gain, and K_d the derivative gain. T_n is the parameter of the derivative filter time constant. The hydroelectric simulator considered in this work exploits an electric servomotor that is used as a governor. The same simulator was already proposed by the authors but with different purposes in [29].

The servomechanism implemented in the hydroelectric simulator is described as a first–order model, which relates the control signal u with the wicket gate servomotor stroke y according to Eq. (23) [30]:

$$\frac{y}{u} = \frac{1}{T_y\, s + 1} \tag{23}$$

with T_y representing the wicket gate servomotor response time.

This concludes the description of the complete nonlinear simulator of a typical hydroelectric plant consisting of two surge tanks and a Francis hydraulic turbine, as represented in Fig. 3.

Note finally that the nonlinear behaviour of the Francis hydraulic turbine and the inelastic water hammer effects were taken into account to compute and simulate realistic hydraulic transients. Due to its nonlinear characteristics, traditional regulation techniques can rely on conventional controllers implementing on–off strategies. Standard PID controllers are also considered for their relative simplicity. However, as remarked *e.g.* in [30] and by the authors in their earlier work [11], classic control solutions can produce unsatisfactory responses, with high overshoot and long settling time.

 doi:10.20944/preprints201810.0572.v1

Moreover, the tuning of the regulator parameters is difficult, as highlighted in [30], since a gain scheduling of the PID parameters would have been required. Thus, advanced control strategies that were already proposed for the wind turbine benchmark and recalled in Section 3 will be briefly summarised and applied to the hydroelectric simulator, as shown in Section 4. Extended simulations, comparisons, and the sensitivity analysis of the proposed solutions represent one of the key points of this paper.

Finally, it is worth noting that some relations of the hydroelectric system have been linearised, see *e.g.* Eqs. (7) and (17). However, this simplified model has been considered for comparison purpose, as the nonlinear parts of the processes under investigation are closer, as highlighted by Eqs. (1) and (15).

3. Advanced Control Techniques for Energy Conversion Systems

This section revises the main control issues and objectives that can be valid for both wind turbine and hydroelectric processes, whilst Section 3.1 summarises those self–tuning control methodologies that will be designed and compared when applied to the considered energy conversion benchmark and simulator.

In general, control systems exploit design algorithms that force a dynamic model to track prescribed references or set–point, such that fixed objectives or behaviour modes are achieved. In this way, the classic control problem is formulated as tracking task, where the system output has to follow the set–point, thus representing the final objective. Tasks expressed in this form are also present in energy conversion applications, for example the speed control of both wind and hydraulic turbines. However, it could be useful to improve the problem descriptions and to give a deeper insight into possible solutions, in order to achieve all potentials of control theory when applied to energy conversion systems.

The complete definition of the control problem usually requires the optimisation of a given prescribed performance index (such as the maximum energy conversion, the minimum power loss) subjected to suitable physical constraints (*e.g.* saturations, amplitudes, rates, forces, torques, etc), thus leading to a constrained minimisation or maximisation problem. The considerations raised here agree with the aim of a standard controlled system including a feedback loop. In fact, the objective index usually represents some metrics (the most common is the quadratic one) of the difference between the reference (*i.e.* the desired value) with respect to the controlled output. This is the well–known tracking error of the monitored output with respect to the set–point. Therefore, the desired behaviour of the controlled process in closed–loop is usually defined in several ways, which represent also the working principles of the control techniques recalled in Section 3.1. First, with reference to the process output, the desired transient or steady–state responses can be considered, as for the case of self–tuning PID regulators summarised in Section 3.1.1. On the other hand, if the frequency behaviour is taken into account, the desired closed–loop poles can be fixed as roots of the closed–loop transfer function. This represent the design approach used by the adaptive strategy considered in Section 3.1.3. Moreover, when robust performances are included, the minimisation of the sensitivity of the closed–loop system with respect to the model–reality mismatch or external disturbances can be considered. This approach is related for example to the fuzzy logic methodology reported in Section 3.1.2. Furthermore, for the case of optimal control, the trade–off between control energy and tracking error has to be evaluated. Control issues related to the model–reality mismatch and the disturbance sensitivity concern the system robustness and reliability. Specific control strategies addressing these objectives have been proposed since the late 1970's. In general, the proposed design methodologies lead to explicit solution for the feedback control laws. Some other strategies provide solutions to this optimisation problem when it is defined at each time step, as for the case of the Model Predictive Control (MPC) with disturbance decoupling considered in Section 3.1.4. The considered strategy integrates the advantages of the MPC solution with the disturbance compensation feature. Therefore, different data–driven and model–based control solutions that may be successfully used for the control

Preprints (www.preprints.org) | NOT PEER-REVIEWED | Posted: 24 October 2018 doi:10.20944/preprints201810.0572.v1

of both the wind turbine benchmark and the hydroelectric plant simulator will be recalled in Section 3.1.

Under these considerations, the general control principle followed in this paper is sketched in Fig. 5. It consists of the optimal set–point generation and the closed–loop design to achieve the reference tracking. These two phases have to take into account of the system physical constraints. For example, the wind turbine system relies on a variable speed turbine, which requires the computation of the optimal rotational speed (ω_r or ω_g) for the regions 1 and 2 of the power curve reported in Fig. 2 (b). Moreover, the reference torque τ_r and the blade pitch control β are also exploited to obtain the needed rotational velocity ω_g. On the other hand, the hydroelectric system requires an optimal velocity reference n_r that is obtained for this plant, and the control of u and y allows to track n according to the desired value n_r. Moreover, the relation of Eq. (16) highlights that the non–dimensional turbine torque M depends on the water flow rate Q, the water level H and the rotational speed n. Furthermore, by including the relation of Eq. (15), the turbine torque M results a function of the water flow rate Q, the rotational speed n and wicked gate opening G.

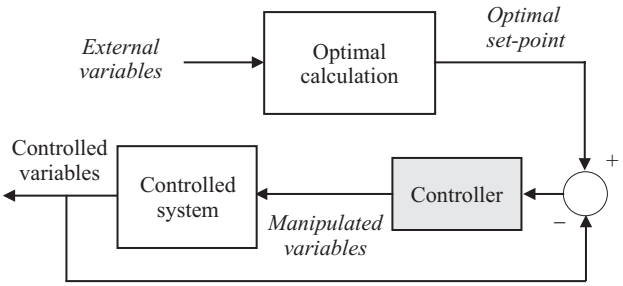

Figure 5. Reference computation for the general closed–loop scheme.

Finally, it is worth noting that model–based control designs rely on the mathematical descriptions of the process models, in order to derive the control laws. The design of standard PID regulators and Model Predictive Control (MPC) methods follows a model–based approach, which will be illustrated in Sections 3.1.1 and 3.1.4, respectively. However, the need for these high–fidelity mathematical descriptions can require much more effort than the derivation of the controller models. Therefore, dynamic system identification methodologies have been successfully proposed in order to determine the so–called black–box or gray–box representations, as addressed *e.g.* in [34], which is also used for the self–tuning PID design. Usually, these descriptions do not present structural relationships to the physical processes. On the other hand, dynamic system identification schemes can be also exploited for deriving adaptive controller prototypes, which are thus able to adapt themselves with respect to unknown conditions or time–varying systems. By means of this 'self–tuning mode', adaptive control strategies relying on linear models of the controlled process are also able to track changes of the plant. Examples of these data–driven approaches are represented by the fuzzy logic and adaptive controllers recalled in Sections 3.1.2 and 3.1.3, respectively. On the other hand, the MPC strategy exploits the proposed disturbance compensation method, which is thus able to cope with uncertainty and model–reality mismatch effects. Note however that, in general, the optimal regulation of nonlinear systems is achieved via purely nonlinear controllers [35]. The stability and convergence properties achieved by the use of adaptive controllers should be carefully analysed over all operating conditions, as addressed in [14]

3.1. Data–Driven and Model–Based Control Methodologies

This section describes briefly several control schemes consisting of self–tuning PID controllers, and Artificial Intelligence (AI) strategies, such as fuzzy logic and adaptive methods, as well as Model Predictive Control (MPC) approach. Some of them were already proposed by the authors for the

Preprints (www.preprints.org) | NOT PEER-REVIEWED | Posted: 24 October 2018 doi:10.20944/preprints201810.0572.v1

application to wind turbine and wind park installations, *e.g.* in [34]. These methodologies will be applied, compared and discussed in Section 4, when considered for both the wind turbine benchmark and the hydraulic plant simulator.

In general, the mathematical formulation of the control law can be provided as linear or nonlinear dynamic function $\mathcal{F}$ in the form of Eq. (24):

$$u(t) = \mathcal{F}\left(y(t)\right) \tag{24}$$

with $y(t)$ being the monitored output, whilst $u(t)$ is the control input. The control techniques proposed for the systems under investigation should lead to the computation of the control law of Eq. (24) generating the input $u(t)$ that allows to track the given reference or set–point $r(t)$ for the controlled output $y(t)$.

Finally, the implementation of the different control techniques is sketched below.

3.1.1. Autotuning Model–Based PID Control

Industrial processes commonly exploit closed–loop including standard PID controllers, due to their simple structure and parameter tuning [36]. The control law depends on the tracking error $e(t)$ defined by the difference between the desired and the measured output signals, *i.e.* $e(t) = r(t) - x(t)$. This signal is injected into the controlled process after proportional, integral and derivative computations. Therefore, the continuous–time control signal $u(t)$ is generated by the PID regulator in the form of Eq. (25):

$$u(t) = K_p\, e(t) + K_i \int_0^t e(\tau)\, d\tau + K_d \frac{de(t)}{dt} \tag{25}$$

with K_p, K_i, K_d being the PID proportional, integral, and derivative gains, respectively. The most common strategy exploited for the computation of the optimal parameters of the PID governor uses proper Ziegler–Nichols formulas, as described in [36]. However, with the development of relatively recent automatic software routines, the PID optimal parameters can be easily determined by means of direct tuning algorithms implemented for example in the Simulink environment. These strategies require the definition of the controlled process as Simulink model, such that they balance the input–output performances of the monitored system in terms of response time and stability margins (robustness) [36]. In particular, the PID automatic tuning procedure implemented in the Simulink toolbox performs the computation of the linearised model of the energy conversion systems studied in this paper. The logic scheme of this procedure is sketched in Fig. 6.

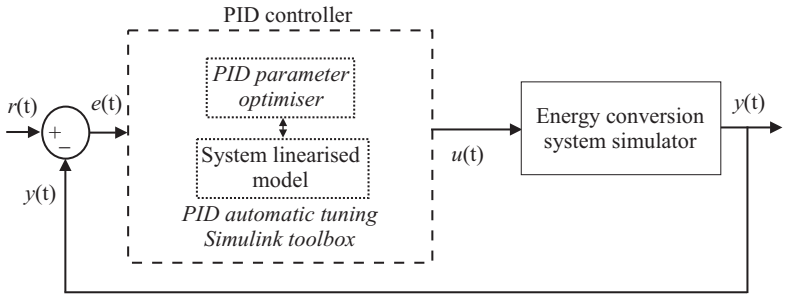

Figure 6. Block diagram of the monitored system controlled by the PID regulator with automatic tuning.

Note finally that the PID block in Fig. 6 performs the computation of a linearised model of the controlled system, if required. Therefore, the optimiser included in the PID block and implemented in the Simulink environment derives of the PID parameters that minimise suitable performance indices, as described in [36].

Preprints (www.preprints.org) | NOT PEER-REVIEWED | Posted: 24 October 2018 doi:10.20944/preprints201810.0572.v1

3.1.2. Data–Driven Fuzzy Logic Control

Fuzzy Logic Control (FLC) solutions are often exploited when the dynamics of the monitored process are uncertain and can present nonlinear characteristics. The design method proposed in this work exploits the direct identification of rule–based Takagi–Sugeno (TS) fuzzy prototypes. Moreover, the fuzzy model structure, *i.e.* the number of rules, the antecedents, the consequents and the fuzzy membership functions can be estimated by means of the Adaptive Neuro–Fuzzy Inference System (ANFIS) toolbox implemented in the Simulink environment [37]. The authors already suggested to employ regulators in the form of TS fuzzy models for designing fault diagnosis and fault tolerant control strategies presented *e.g.* in [29].

The TS fuzzy prototype relies on a number of rules R_i, whose consequents are deterministic functions $f_i(\cdot)$ in the form of Eq. (26):

$$R_i : IF\ x\ is\ A_i\ THEN\ u_i = f_i(x) \tag{26}$$

where the index $i = 1, 2, \ldots, K$ describes the number of rules K, x is the input vector containing the antecedent variables, *i.e.* the model inputs, whilst u_i represents the consequent output. The fuzzy set A_i describing the antecedents in the i–th rule is described by its (multivariable) membership function $\mu_{A_i}(x) \rightarrow [0, 1]$. The relation $f_i(x)$ assumes the form of parametric affine model represented by the i–th relation of Eq. (27):

$$u_i = a_i^T\, x + b_i \tag{27}$$

with the vector a_i and the scalar b_i being the i–th submodel parameters. The vector x consists of a proper number n of delayed samples of input and output signals acquired from the monitored process. Therefore, the term $a_i^T\, x$ is an Auto–Regressive eXogenous (ARX) parametric dynamic model of order n, and b_i a bias.

The output u of the TS fuzzy prototype is computed as weighted average of all rule outputs u_i in the form of Eq. (28):

$$u = \frac{\sum_{i=1}^{K} \mu_{A_i}(x)\, y_i(x)}{\sum_{i=1}^{K} \mu_{A_i}(x)} \tag{28}$$

The estimation scheme implemented by the ANFIS tool follows the classic dynamic system identification experiment. First, the structure of the TS fuzzy prototype is defined by selecting a suitable order n, the shape representing the membership functions μ_{A_i}, and the proper number of clusters K. Therefore, the input–output data sequences acquired from the monitored system are exploited by ANFIS for estimating the TS model parameters and its rules R_i after the selection of a suitable error criterion. The optimal values of the controller parameters represented by the variables a_i and b_i of (27) are thus estimated [38].

The work proposes also a strategy different from ANFIS that can be exploited for the estimation of the parameters of the fuzzy controller. This method relies on the Fuzzy Modelling and Identification (FMID) toolbox designed in the Matlab and Simulink environments as described in [39]. Again, the computation of the controller model is performed by estimating the rule–based fuzzy system in the form of Eq. (28) from the input–output data acquired from the process under investigation. In particular, the FMID tool uses the Gustafson–Kessel (GK) clustering method [39] to perform a partition of input–output data into a proper number K of regions where the local affine relations of Eq. (27) are valid. Also in this case, the fuzzy controller model of Eq. (28) is computed after the selection of the model order n and the number of clusters K. The FMID toolbox derives the variables a_i and b_i, as well as the identification of the shape of the functions μ_{A_i} by minimising a given metric [39].

Note that the overall digital control scheme consisting of the discrete–time fuzzy regulator of Eq. (28) and continuous–time nonlinear system of Eq. (24) includes also Digital–to–Analog (D/A) and Analog–to-Digital (A/D) converters, as shown in Figure 7.

Preprints (www.preprints.org) | NOT PEER-REVIEWED | Posted: 24 October 2018 doi:10.20944/preprints201810.0572.v1

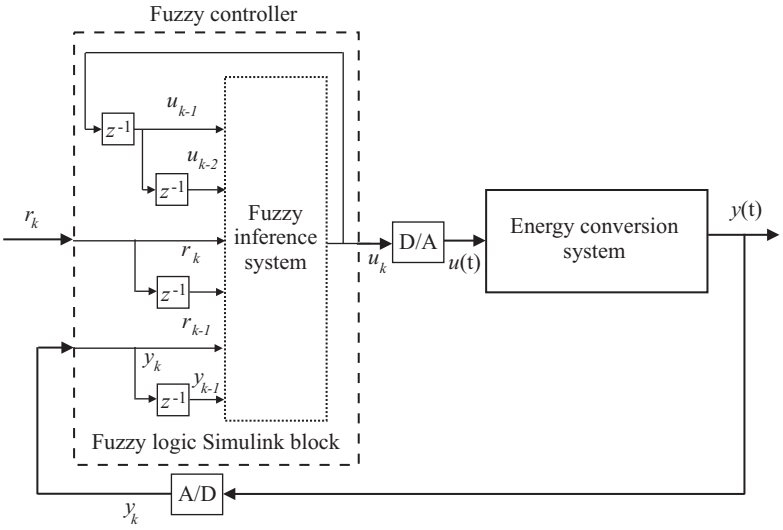

Figure 7. Block diagram of the monitored system controlled by the fuzzy regulator.

With reference to Figure 7, note finally that the fuzzy controller block implemented in the Simulink environment includes a suitable number n of delayed samples of the signals acquired from the monitored process. Moreover, the fuzzy inference system in Figure 7 implements the TS model of Eq. (28). The delay n, the membership functions μ_{A_i}, and the number of clusters K are estimated by the FMID and the ANFIS toolboxes, as described in [39].

3.1.3. Data–Driven Adaptive Control

The adaptive control technique proposed in this work relies on the recursive estimation of a 2–nd order discrete–time transfer function $G(z)$ with time–varying parameters described by Eq. (29):

$$G(z) = \frac{\beta_1 z^{-1} + \beta_2 z^{-2}}{1 + \alpha_1 z^{-1} + \alpha_2 z^{-2}} \tag{29}$$

where α_i and β_i are identified on–line at each sampling time $t_k = k\,T$, with $k = 1, 2, \ldots, N$, for N samples, and T being the sampling interval. z^{-1} indicates the unit delay operator. A viable and direct way for deriving the model parameters in Eq. (29) that is proposed in this work is based on the Recursive Least–Square Method (RLSM) with directional forgetting factor, which was presented in [40]. Note that the authors suggested to use on–line techniques also for the development of fault tolerant control system, as described in [29].

Once the parameters of the model of Eq. (29) have been derived, this paper proposes to compute the adaptive controller in the form of Eq. (30):

$$u_k = q_0\, e_k + q_1\, e_{k-1} + q_2\, e_{k-2} + (1 - \gamma)\, u_{k-1} + \gamma\, u_{k-2} \tag{30}$$

with e_k and u_k represent the sampled values of the tracking error $e(t)$ and the control signal u_k at the time t_k, respectively. With reference to the description of Eq. (30), by following a modified Ziegler–Nichols criterion, q_0, q_1, q_2, and γ represent the adaptive controller parameters, which are

Preprints (www.preprints.org) | NOT PEER-REVIEWED | Posted: 24 October 2018 doi:10.20944/preprints201810.0572.v1

derived by solving a Diophantine equation. As described in [40], by considering the recursive 2–nd order model of Eq. (29), this technique leads to the relations of Eqs. (31):

$$\begin{cases} q_0 &= \frac{1}{\beta_1}\ (d_1 + 1 - \alpha_1 - \gamma) \\ \gamma &= \frac{s_1}{r_1}\ \frac{\beta_2}{\alpha_2} \\ q_1 &= \frac{\alpha_2}{\beta_2} - \frac{s_1}{r_1}\ \left(\frac{\beta_1}{\beta_2} - \frac{\alpha_1}{\alpha_2} + 1\right) \\ q_2 &= \frac{s_1}{r_1} \end{cases} \tag{31}$$

where:

$$\begin{cases} r_1 &= (b_1 + b_2)\ (a_1\, b_2\, b_1 - a_2\, b_1^2 - b_2^2) \\ s_1 &= a_2\ ((b_1 + b_2)\ (a_1\, b_2 - a_2\, b_1) + b_2\ (b_1\, d_2 - b_2\, d_1 - b_2)) \end{cases} \tag{32}$$

Note that the design technique proposed in this work and represented by the relations of Eqs. (31) and (32) assumes that the behaviour of the overall closed–loop system can be approximated by a 2nd order transfer function with characteristic polynomial represented by Eq. (33):

$$D(s) = s^2 + 2\,\delta\,\omega\,s + \omega^2 \tag{33}$$

with δ and ω being the damping factor and natural frequency, respectively. s is the derivative operator. Furthermore, if $\delta \leq 1$, the following relations are used [40]:

$$\begin{cases} d_1 &= -2\,e^{-\delta\,\omega\,T}\ \cos\left(\omega\,T\sqrt{1-\delta^2}\right) \\ d_2 &= e^{-2\,\delta\,\omega\,T} \end{cases} \tag{34}$$

This paper suggested this adaptive control technique since both the recursive estimation procedure of Eq. (29) and the on–line computation of the control law of Eq. (30) are available from the digital Self–Tuning Controller Simulink Library (STCSL) described in [40]. According to this solution, the output y_k of the time–varying model of Eq. (29) follows the reference signal r_k when the control law of Eq. (30) is . The achievable performances depend on the design parameters given by Eq. (33).

The on–line control law of Eq. (30) is used for the regulation of the continuous–time nonlinear system of Eq. (24) by including D/A and A/D converters, as highlighted in the scheme of Figure 8.

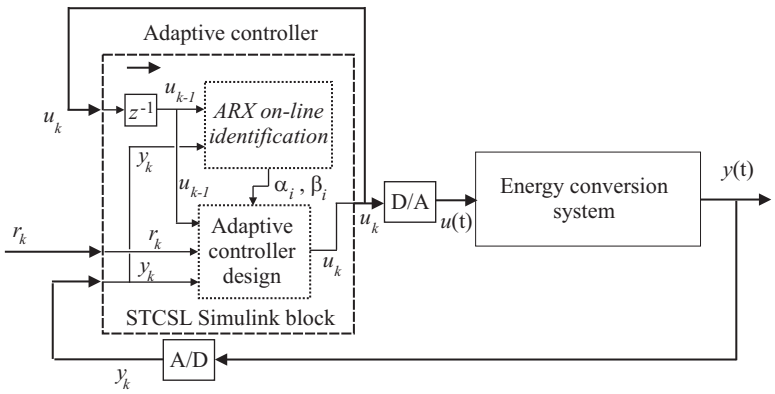

Figure 8. Block diagram of the monitored system controlled by the adaptive regulator.

Preprints (www.preprints.org) | NOT PEER-REVIEWED | Posted: 24 October 2018 doi:10.20944/preprints201810.0572.v1

Note finally that the adaptive control sketched in Figure 8 is implemented via the STCSL block in the Simulink environment. It includes the module performing the on–line identification of the ARX model of Eq. (29), which is used for the adaptive controller design in the form of Eq. (30) [40].

3.1.4. MPC with Disturbance Decoupling

The general structure of the proposed MPC is illustrated in Figure 9, with the MPC managing objectives and constraints of the control inputs. The MPC works as a standard MPC controller when the nominal plant is considered, and generates the reference inputs. In the presence of disturbance or uncertainty effects, the considered solution provides the reconstruction of the equivalent disturbance signal acting on the plant. This represent the key feature of this structure, which compensates the disturbance effect and 'hide' it to the overall system. In this way, it decouples the disturbance effect from the nominal MPC design. Another feature of this structure is the management of the objectives and constraints through the MPC design. These objective and constraints can be the nominal ones. But in case of disturbance or uncertainty, when the nominal performance cannot be achieved, the objectives could be switched to degraded ones and the constraints can also be updated if necessary. The powerful tool to achieve the required fault tolerance characteristic is the optimisation lying in the MPC design itself.

The overall scheme is thus represented aim by the MPC design with disturbance compensation, such that the compensated system has response very similar to the nominal system and the constraints are not violated. The fault compensation problem within the MPC framework is defined as follows. Given a state–space representation of the considered system affected by disturbance or uncertainty has the following form:

$$\begin{cases} \dot{x}_l &= A_l\, x_l + B_l\, u + B_d\, d + w \\ y_l &= C_l\, x_l + v \end{cases} \tag{35}$$

and its nominal reference model:

$$\begin{cases} \dot{x}_r &= A_l\, x_r + B_l\, u_r \\ y_r &= C_l\, x_r \end{cases} \tag{36}$$

the disturbance compensation problem is solved by finding the control input u that minimises the cost function:

$$J = \int_t^{t+N_c\,\Delta t} \left(\|x_l - x_r\|_Q^2 + \|\dot{u}\|_R^2 \right)\, d\tau \tag{37}$$

given the reference input u_r.

In Eq. (35) the matrices A_l, B_l, B_d and C_l are of proper dimensions. The vector y_l represents the output measurements, x_l is the state of the model with disturbance, whilst x_r is the reference state, and y_r the reference output, corresponding to the reference input u_r of the nominal model. The vectors w and v include the model mismatch and the measurement error, respectively. d represents the equivalent disturbance signal. In Eq. (37) t is the current time, Δt is the control interval, and N_c is the length of the control horizon. Q and R are suitable weighting matrices. Note that the model of Eq. (35) can be derived by nonlinear model linearisation or identification procedures, as suggested in Sections 3.1.1 and 3.1.3, respectively.

This work proposes to solve the problem in two steps: the reconstruction of the disturbance d, *i.e.* $\hat{d}$, provided by the disturbance estimation module, and the MPC tool. Due to the model–reality mismatch and the measurement error in (35), the Kalman filter (38) is used to provide the estimation of the state vector x_l, the output y_l of the system affected by the estimated disturbance $\hat{d}$:

$$\begin{cases} \dot{x}_l &= A_l\, x_l + B_l\, u - B_l\, \hat{d} + K_f\, (y_l - C_l\, x_l) \\ y_l &= C_l\, x_l \end{cases} \tag{38}$$

Preprints (www.preprints.org) | NOT PEER-REVIEWED | Posted: 24 October 2018 doi:10.20944/preprints201810.0572.v1

where K_f is the Kalman filter gain. In this way, based on the estimations $\hat{d}$ and x_l, an MPC is designed, which contains the reference model of Eq. (36) and the filtered system of Eq. (38), with $\hat{d}$ provided by the Kalman filter. Moreover, the MPC has the objective function:

$$\int_t^{t+N_c\,\Delta t} \left[(x_l - x_r)^T \; Q \; (x_l - x_r) + \dot{u}^T \, R \, \dot{u} \right] d\tau \tag{39}$$

in which x_l and x_r are the states of the filtered and the reference models, respectively. The integrated MPC with the Kalman filter solves this general disturbance compensation problem, as long as the estimations of both the state and the disturbance are correct. An illustration of the structure of the fault compensated MPC is shown in Figure 9.

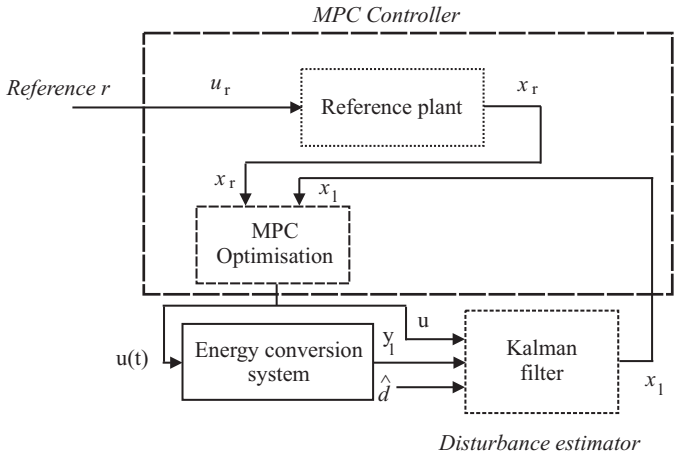

Figure 9. Block diagram of the monitored system controlled via the disturbance compensated MPC scheme.

The global estimation and control scheme is a nonlinear MPC problem with the nominal model for the considered energy conversion systems of Eq. (35), the disturbance d with its estimator, and the Kalman filter of Eq. (38) as prediction model. The local observability of the model of Eq. (35) is essential for state estimation, which is easily verified. The implementation of the proposed disturbance compensation strategy has been integrated into the MPC Toolbox of the Simulink environment.

Note finally that the authors applied the MPC technique to the Fault Tolerant Control (FTC) framework in [41].

4. Results, Comparisons and Discussions

This work recalled different control techniques as reported in Section 3 that are proposed to compensate the outputs of both the wind turbine benchmark and the hydroelectric plant simulator summarised in Section 2. On the other hand, this section presents the simulations achieved in the Matlab and Simulink environments implementing these control techniques by means of the tools recalled in Section 3.1. The obtained results are evaluated via the percent Normalised Sum of Squared Error ($NSSE\%$) performance function in the form of Eq. (40):

$$NSSE\% = 100 \sqrt{\frac{\sum_{k=1}^{N} (r_k - o_k)^2}{\sum_{k=1}^{N} r_k^2}} \tag{40}$$

with r_k being the sampled reference or set–point $r(t)$, whilst o_k is the sampled continuous–time signal representing the generic controlled output $y(t)$ of the process. In particular, this signal is represented

Preprints (www.preprints.org) | NOT PEER-REVIEWED | Posted: 24 October 2018 doi:10.20944/preprints201810.0572.v1

by the wind turbine generator angular velocity $\omega_g(t)$ in Eq. (3), and the hydraulic turbine rotational speed n in Eq. (19) for the hydroelectric plant.

Note that the wind turbine benchmark and the hydroelectric plant simulator of Section 2 allow the generation of several input–output data sequences due to different wind speed $v(t)$ effects (see *e.g.* (1)) and hydraulic transient under variable loads m_{g0} (see *e.g.* (21)), respectively. Moreover, in order to obtain comparable working situations, the wind turbine benchmark has been operating from partial to full load conditions, as highlighted in Figure 2 (b). It is thus considered the similar maneuver of the hydroelectric system operating from the start–up to full load working condition. After these considerations, Section 4.1 summarises the results obtained from the wind turbine benchmark first. Then, the same control techniques will be verified when applied to the hydroelectric simulator.

It is worth highlighting that the simulations considered in this work take into account disturbance and uncertainty effects. In fact, the hydroelectric plant considers a load disturbance, whilst the turbine simulator is driven by wind, which represents the main disturbance source. Moreover, the uncertainty effect has been analysed in Section 4.2.

4.1. Control Technique Performances and Comparisons

Figure 10 reports the results achieved with the control methodologies and the tools summarised in Section 3.1. In particular, Figure 10 depicts the wind turbine generator angular velocity ω_g when the wind speed $v(t)$ changes from 3 m/s to 18 m/s for a simulation time of 4400*s*. This simulation time is defined by the wind turbine benchmark in [10,42] using a real wind sequence sampled for 4400*s*. Moreover, the initial value of the signal ω_g is different from zero since the simulation commences when the wind speed has already exceeded the cut–in value highlighted in Figure 2 (b).

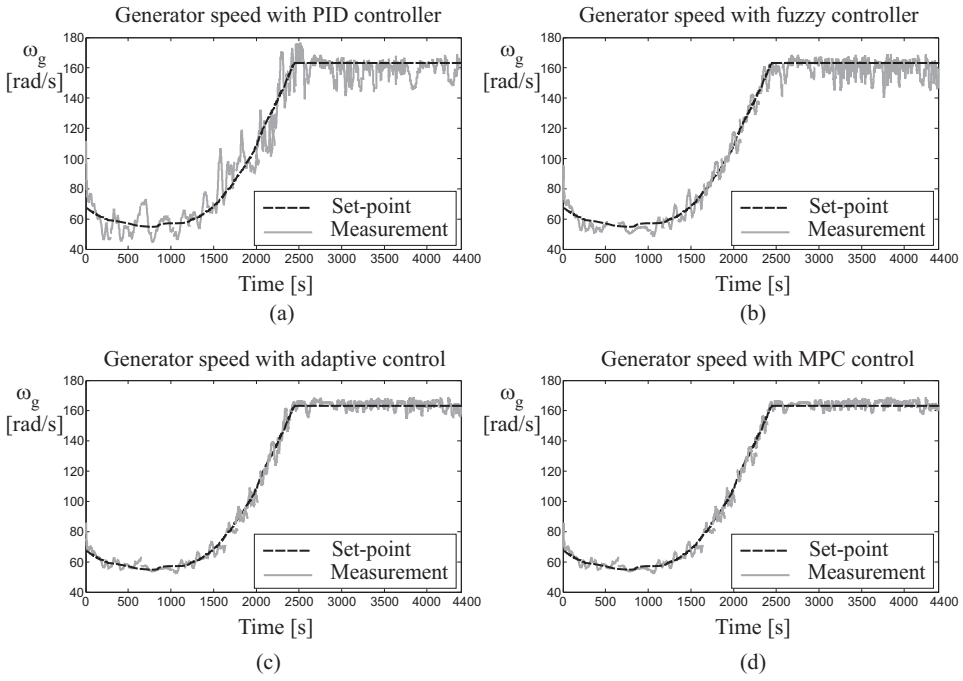

Figure 10. Wind turbine controlled output compensated by (a) the autotuning PID regulator, (b) the fuzzy controller, (c) the adaptive regulator, and (d) the MPC approach with disturbance decoupling.

In detail, with reference to the picture in Figure 10 (a), the parameters of the PID regulator of Eq. (25) have been determined using the model–based autotuning tool available in the Matlab and Simulink environments. They were settled to $K_p = 4.0234$, $K_i = 1.0236$, $K_d = 0.0127$, as described in Section 3.1.1. The achieved performances are better than the ones obtained with the baseline control laws proposed in [10] and recalled in Section 2.1.

Preprints (www.preprints.org) | NOT PEER-REVIEWED | Posted: 24 October 2018 doi:10.20944/preprints201810.0572.v1

Moreover, Figure 10 (b) shows the simulations achieved with the data–driven fuzzy identification approach recalled in Section 3.1.2. This strategy was proposed here since it represents a viable and practical way for deriving the models of the controllers by means of the so–called model reference control approach, as addressed in [43]. According to this strategy, the baseline PID regulators designed for the nominal wind turbine model were considered as reference controllers for the generation of the input–output data used by the identification methodology recalled in Section 3.1.2. In this way, the TS fuzzy controller parameters are estimated such that they optimise the performances in terms of tracking error. In particular, a sampling interval $T = 0.01s$ has been exploited, and the TS fuzzy controller of Eq. (28) has been obtained for a number $K = 3$ of Gaussian membership functions, and a number $n = 2$ of delayed inputs and output. The antecedent vector in Eq. (27) is thus $x = [e_k, e_{k-1}, e_{k-2}, u_{k-1}, u_{k-2}]$. Both the data–driven FMID and ANFIS tools available in the Matlab and Simulink environments provide also the optimal identification of the shapes of the fuzzy membership functions μ_{A_i} of the fuzzy sets A_i in Eq. (26).

On the other hand, the picture in Figure 10 (c) shows the capabilities of the adaptive controller of Eq. (30). The time–varying parameters of this data–driven control technique summarised in Section 3.1.3 have been computed on–line via the relations of Eqs. (31) with the damping factor and the natural frequency variables $\delta = \omega = 1$ in Eq. (33). As already remarked, this work considered this data–driven adaptive technique since it was already implemented in the Simulink environment via the Self Tuning Controller Simulink Library (STCSL) [40].

Finally, the picture of Figure 10 (d) highlights the results achieved with the MPC technique with disturbance decoupling recalled in Section 3.1.4. The state–space model of the wind turbine nonlinear system of Eq. (3) exploited for the design of the MPC and the Kalman filter for the estimation of the disturbance has order $n = 5$, with a prediction horizon $N_p = 10$ and a control horizon $N_c = 2$. The weighting factors have been settled to $w_{y_k} = 0.1$ and $w_{u_k} = 1$, in order to reduce possible abrupt changes of the control input. Note that, in this case, the MPC technique has led to the best results, since it exploits a disturbance decoupling strategy, whilst its parameters have been iteratively adapted in the Simulink environment in order to optimise the MPC cost function of Eq. (37), as addressed in Section 3.1.4.

The second test case regards the hydroelectric plant simulator, where the hydraulic system with its turbine speed governor generates hydraulic transients due to the load changes. As already recalled in Section 2.2, an effective behaviour of a classic PID governor addressed *e.g.* in [30] applied to this hydroelectric plant would require the scheduling of its gains. In such a way only the performance of this standard controller could have been improved. In fact, in order to obtain the best dynamic performance of the hydraulic turbine, the PID governor of the turbine speed in Eq. (22) should consider different parameters for each working condition. Therefore, in order to consider operating situations similar to the wind turbine benchmark, the capabilities of the considered control techniques applied to the hydroelectric simulator have been evaluated during the start–up to full load maneuver. Moreover, an increasing load torque m_{g0} in Eq. (21) has been imposed during the start–up to full load phase, which is assumed to last $300s$ because of the large size of the considered Francis turbine, and for a simulation of $900s$. This represents one of the different working conditions already addressed by the authors in [29] but for fault diagnosis applications. It is worth noting that these slow varying set–points have been considered for comparison purpose. In fact, as shown in [21], the wind turbine simulator presents similar dynamics, as highlighted in Figure 10.

Under these assumptions, Figure 11 summarises the results achieved with the application of the control strategies recalled in Section 3.1. In particular, for all cases, Figure 11 highlights that the hydraulic turbine angular velocity n increases with the load torque m_{g0} during the start–up to full working condition maneuver.

In more detail, Figure 11 (a) shows the performance of the PID regulator when its parameters are determined via the model–based autotuning procedure recalled in Section 3.1.1. In particular, its gains are determined with the algorithm implemented in the Simulink environment. It tries to

Preprints (www.preprints.org) | NOT PEER-REVIEWED | Posted: 24 October 2018 doi:10.20944/preprints201810.0572.v1

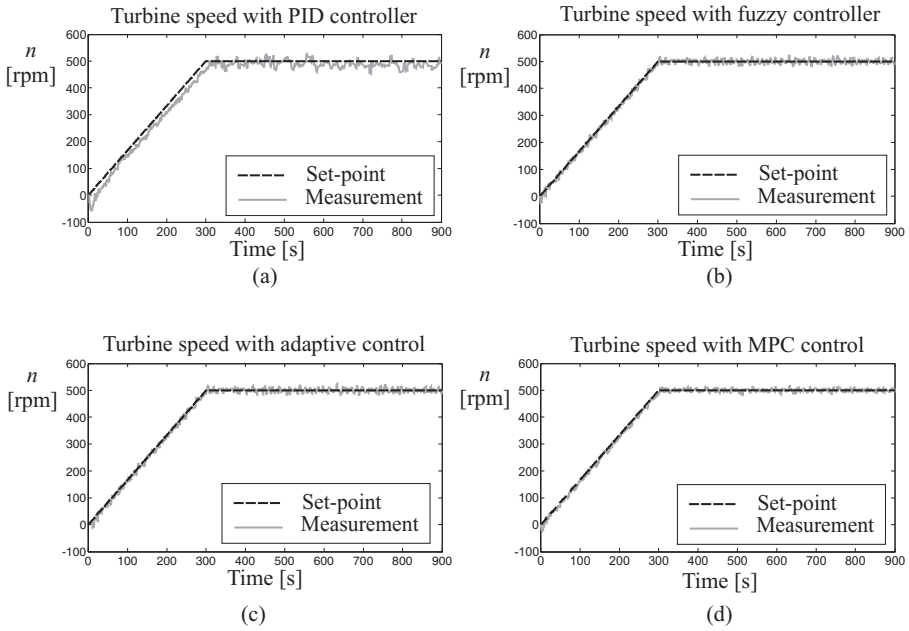

Figure 11. Hydroelectric system with (a) the autotuning PID regulator, (b) the fuzzy controller, (c) the adaptive regulator, and (d) the MPC approach with disturbance decoupling.

compute in an automatic way the optimal parameters of the PID regulator that minimise the step response tracking error of the linear model approximating the nonlinear behaviour of the hydraulic plant. Furthermore, Figure 11 (a) shows that the PID governor with autotuning is able to keep the hydraulic turbine rotational speed error $n - n_r$ null ($r(t) = n_r$, *i.e.* the rotational speed constant) in steady–state conditions.

Figure 11 (b) reports the results concerning the TS fuzzy controller described by Eq. (28) in Section 3.1.2. This fuzzy controller was implemented for a sampling interval $T = 0.1s$, with a number $K = 2$ of Gaussian membership functions, and a number $n = 3$ of delayed inputs and output. The antecedent vector exploited by the relation of Eq. (27) is thus $x = [e_k, e_{k-1}, e_{k-2}, e_{k-3}, u_{k-1}, u_{k-2}, u_{k-3},]$. Moreover, as recalled in Section 3.1.2, the data–driven FMID and ANFIS tools implemented in the Simulink toolboxes are able to provide the estimates of the shapes of the membership functions μ_{A_i} used in Eq. (28).

On the other hand, Figure 11 (c) reports the simulations obtained via the data–driven adaptive controller of Eq. (30), whose time–varying parameters are computed by means of the relations of Eqs. (31). The damping factor and the natural frequency parameters used in Eq. (33) were selected as $\delta = \omega = 1$. The STCSL tool described in Section 3.1.3 implements this data–driven adaptive technique using the on–line identification of the input–output model of Eq. (29) [40].

Finally, regarding the MPC technique with disturbance decoupling proposed in Section 3.1.4, Fig. 11 (d) reports the simulations obtained using a prediction horizon $N_p = 10$ and a control horizon $N_c = 2$. Also in this case, the weighting parameters have been fixed to $w_{y_k} = 0.1$ and $w_{u_k} = 1$, in order to limit fast variations of the control input, as it will be remarked in the following. Furthermore, the MPC design was performed using a linear state–space model for the nonlinear hydroelectric plant simulator of Eq. (24) of order $n = 6$.

After these considerations, it is worth noting that some of the control techniques recalled in this paper rely on self–tuning and adaptive methodologies, that are based on data–driven algorithms. This means that they do not need for the knowledge of a high–fidelity description of the controlled process, thus providing a viable and direct implementation. Some of these strategies were analysed in [16] with application to general hydroelectric plant models, but implemented by using different

Preprints (www.preprints.org) | NOT PEER-REVIEWED | Posted: 24 October 2018 doi:10.20944/preprints201810.0572.v1

algorithms. Moreover, as an example, the work [44] presented a fuzzy controller that needs for the proper design of the membership functions. On the other hand, the paper [17] proposed an advanced controller combining four control schemes that rely on adaptive, fuzzy and neural network regulators.

In order to provide a quantitative comparison of the tracking capabilities obtained by the considered control techniques for the wind turbine benchmark, the first row in Table 3 summarises the achieved results in terms of $NSSE\%$ index.

Table 3. Performance of the considered control solutions.

Simulated system	Working Condition	Standard PID	Autotuning PID	Fuzzy PID	Adaptive PID	MPC Scheme
Wind turbine	From partial to full load	11.5%	7.3%	5.7%	4.1%	2.8%
Hydro plant	From start–up to full load	6.2%	4.9%	3.1%	1.8%	0.9%

In particular, the $NSSE\%$ values in the first row of Table 3 highlight better capabilities of the proposed fuzzy controllers with respect to the PID regulators with autotuning. This is motivated by the better flexibility and generalisation capabilities of the fuzzy tool, and in particular the FMID toolbox proposed in [39]. A better behaviour is obtained by means of the adaptive solution, due to its inherent adaptation mechanism, which allows to track the reference signal in the different working conditions of the wind turbine process. However, the MPC technique with disturbance decoupling has led to the best results, as reported in the first row of Table 3, since is able to optimise the overall control law over the operating conditions of the system, by taking into account future operating situations of its behaviour. while compensating the disturbance effects.

On the other hand, the results achieved by the validation of the considered control techniques to the hydroelectric plant simulator are summarised in the second row of Table 3. In this case, the values of the $NSSE\%$ function are evaluated for the considered conditions of varying load torque m_{g0} corresponding to the plant start–up to full load maneuver. According to these simulation results, good properties of the proposed model–based autotuning PID regulator are obtained, and they are better than the baseline PID governor with fixed gains developed in [30]. In fact, the autotuning model–based design implemented in the Simulink environment is able to limit the effect of high–gains for the proportional and the integral contributions of the standard PID control law. On the other hand, the data–driven fuzzy regulator has led to even better results, which are outperformed by the adaptive solution. However, also for the case of the hydroelectric plant simulator, the best performances are obtained by means of the MPC strategy with disturbance decoupling. Note that, with reference to Table 3, the comparison should be performed by considering the $NSSE\%$ values for a given plant. In fact, even if the $NSSE\%$ index assumes quite similar values, it refers to control techniques implemented and applied to different processes.

With reference again to Table 3, some further comments can be drawn in general, concerning the key aspects of the considered data–driven and model–based control solutions, with respect to the standard PID regulators. The $NSSE\%$ values obtained here are lower for both the wind turbine and the hydroelectric systems. Standard industrial controllers, such the classic PID regulators recalled in Section 2, are quite simple and have the benefit of quite straightforward tuning of their parameters. Note that these standard regulators are considered here since they were implemented as baseline controllers for the considered processes, see *e.g.* [10,30]. Obviously, when exploited for controlling nonlinear dynamic processes, the control laws may lead to limited performances. Therefore, this point motivates the use of suitable control solutions, as highlighted by the results summarised in Table 3. In particular, when the modelling of the dynamic process can be perfectly achieved, model–based control strategies generally represent the best option. However, when modelling

Preprints (www.preprints.org) | NOT PEER-REVIEWED | Posted: 24 October 2018 doi:10.20944/preprints201810.0572.v1

errors and uncertainty effects are important, data–driven control schemes relying on adaptation or compensation mechanisms can show interesting features.

Finally, in order to highlight some further features of the considered, the controlled inputs applied to the wind turbine system are depicted and compared in Figures 12 (a) and (c), whilst the one feeding the hydroelectric plant in Figure 12 (b) and (d). For the sake of brevity, only the data–driven fuzzy controller and the MPC with disturbance decoupling have been summarised here.

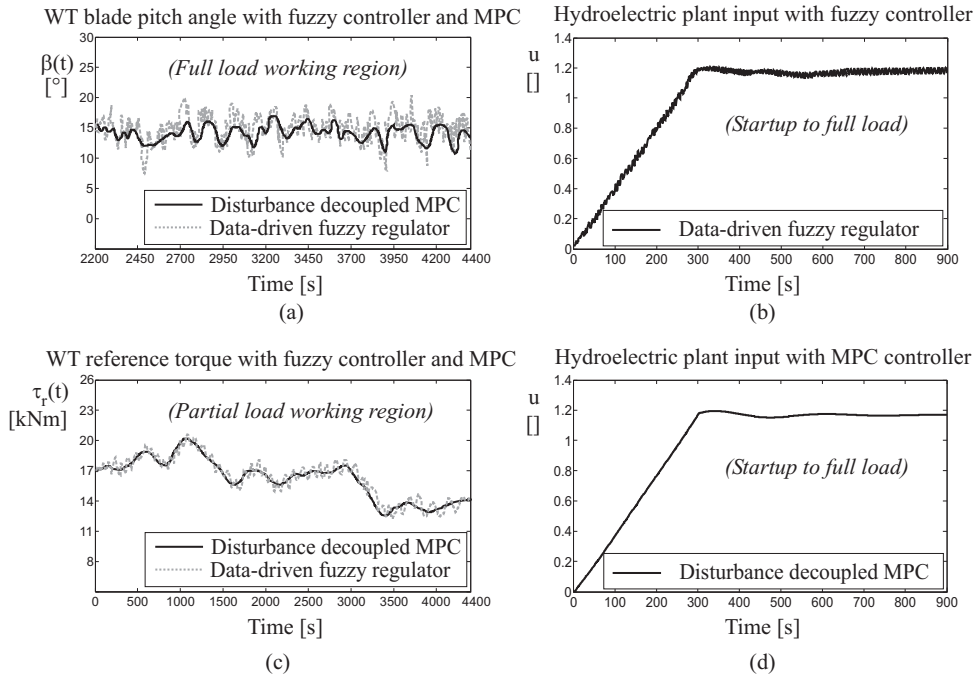

Figure 12. Wind turbine (a), (c) and hydroelectric plant (b), (d) compensated by the fuzzy controller and the MPC approach with disturbance decoupling.

By considering these control inputs, with reference to the data–driven methodologies, and in particular to the design of the fuzzy controllers, off–line optimisation strategies allow to reach quite good results. However, control inputs are subjected to faster variations. Other control techniques can take advantage of more complicated and not direct design methodologies, as highlighted by the MPC scheme. In this case, due to the input constraint, its changes are reduced. This feature is attractive for wind turbine systems, where variations of the control inputs must be limited. This represents another important benefit of MPC with disturbance decoupling, which integrates the advantages of the classic MPC scheme with disturbance compensation effects. Therefore, with reference to these two control methods, they can appear rather straightforward, even if further optimisation and estimation strategies have to be applied.

4.2. Sensitivity Analysis

This section analyses the reliability and robustness properties of the developed controllers when parameter variations and measurement errors are considered. This further investigation relies on the Monte–Carlo tool, since the control behaviour and the tracking capabilities depend on both the model–reality mismatch effects and the input–output uncertainty levels. Therefore, this analysis has been implemented by describing the parameters of both the wind turbine system and hydroelectric plant models as Gaussian stochastic processes with average values corresponding to the nominal ones summarised in Table 4 for the wind turbine benchmark.

Moreover, Table 4 shows that these model parameters have standard deviations of $\pm 30\%$ of the corresponding nominal values [24].

Preprints (www.preprints.org) | NOT PEER-REVIEWED | Posted: 24 October 2018 doi:10.20944/preprints201810.0572.v1

Table 4. Wind turbine benchmark parameters for the sensitivity analysis.

Variable	R	χ	ω_n	B_{dt}	B_r
Nominal value	57.5 m	0.6	11.11 $rad\,s^{-1}$	775.49 $N\,m\,s\,rad^{-1}$	7.11 $N\,m\,s\,rad^{-1}$
Variable	B_g	K_{dt}	η_{dt}	J_g	J_r
Nominal value	45.6 $N\,m\,s\,rad^{-1}$	$2.7 \cdot 10^9$ $N\,m\,rad^{-1}$	0.97	390 $kg\,m^2$	$55 \cdot 10^6$ $kg\,m^2$

On the other hand, Table 5 reports the hydroelectric simulator model variables with their nominal values varied by ±30% in order to develop the same Monte–Carlo analysis [11].

Table 5. Hydroelectric simulator parameters for the sensitivity analysis.

Variable	a	b	c	H_{f_1}	H_{f_3}	H_{f_5}	T_a
Nominal value	-0.08	0.14	0.94	0.0481 m	0.0481 m	0.0047 m	5.9 s
Variable	T_c	T_{s_2}	T_{s_4}	T_{w_1}	T_{w_3}	T_{w_5}	
Nominal value	20 s	476.05 s	5000 s	3.22 s	0.83 s	0.1 s	

Therefore, the average values of $NSSE\%$ index have been thus evaluated by means of 1000 Monte–Carlo simulations. They have been reported in Tables 6 and 7 for the wind turbine benchmark and the hydroelectric plant simulator, respectively.

Table 6. Sensitivity analysis applied to the wind turbine benchmark.

Standard PID	**Autotuning PID**	**Fuzzy PID**	**Adaptive PID**	**MPC Scheme**
13.8%	9.2%	7.6%	5.3%	3.9%

Table 7. Sensitivity analysis applied to the hydroelectric plant simulator.

Standard PID	**Autotuning PID**	**Fuzzy PID**	**Adaptive PID**	**MPC Scheme**
9.1%	7.4%	5.6%	3.5%	2.2%

It is worth noting that the results summarised in Tables 6 and 7 serve to verify and validate the overall behaviour of the developed control techniques, when applied to the considered wind turbine benchmark and hydroelectric plant simulator, respectively. In more detail, the values of the $NSSE\%$ index highlights that when the mathematical description of the controlled dynamic processes can be included in the control design phase, the model–based MPC technique with disturbance decoupling still yields to the best performances, even if an optimisation procedure is required. However, when modelling errors are present, the off–line learning exploited by the data–driven fuzzy regulators allows to achieve results better than model–based schemes. For example, this consideration is valid for the PID controllers derived via the model–based autotuning procedures. On the other hand, fuzzy controllers have led to interesting tracking capabilities. With reference to the data–driven adaptive scheme, it takes advantage of its recursive features, since it is able to track possible variations of the controlled systems, due to operation or model changes. However, it requires quite complicated and not straightforward design procedures relying on data–driven recursive algorithms. Therefore, fuzzy–based schemes use the learning accumulated from data–driven off–line

simulations, but the training stage can be computationally heavy. Finally, concerning the standard PID control model–based strategy, it is rather simple and straightforward. Obviously, the achievable performances are quite limited when applied to nonlinear dynamic processes. Note that they were proposed as baseline control solutions for the considered processes. It can be thus concluded that the proposed data–driven and model–based approaches seem to represent powerful techniques able to cope with uncertainty, disturbance and variable working conditions. Note finally that the plant simulators, the control solutions, and the data exploited for the analysis addressed in this paper are directly and freely available from the authors.

5. Conclusions

The work considered two renewable energy conversion systems, such as a wind turbine benchmark and a hydroelectric plant simulator. The most important modelling aspects and the baseline control strategies were also summarised. In particular, the three–bladed horizontal axis wind turbine benchmark reported in this work consisted of simple models of the gear–box, the drive–train, and the electric generator/converter. On the other hand, the hydroelectric plant simulator included a high water head, a long penstock with upstream and downstream surge tanks, and a Francis hydraulic turbine. Standard PID governors were earlier developed for these processes, which were rather simple and straightforward, but with limited achievable performances. Therefore, the paper proposed different control techniques relying on model–based and data–driven approaches. Their performances were analysed first. Then, the reliability and robustness of these solutions were also verified and validated with respect to parameter variations of the plant models and measurement errors, via the Monte–Carlo tool. The achieved results highlighted that data–driven approaches, such as the fuzzy regulators were able to provide good tracking performances. However, they were easily outperformed by adaptive and model predictive control schemes, representing data–driven and model–based approaches that require optimisation stages, adaptation procedures and disturbance compensation methods. Future investigations will consider the verification and the validation of the considered control techniques when applied to higher fidelity simulators of energy conversion systems.

Sample Availability: The software codes for the proposed control strategies, the simulated benchmarks and the generated data are available from the authors on demand in the Maltab and Simulink environments.

Acknowledgments: The research works have been supported by the FAR2018 local fund from the University of Ferrara. On the other hand, the costs to publish in open access have been covered by the FIR2018 local fund from the University of Ferrara.

Author Contributions: Silvio Simani conceived and designed the simulations. Silvio Simani analysed the methodologies, the achieved results, and together with Stefano Alvisi and Mauro Venturini, wrote the paper.

Conflicts of Interest: The authors declare no conflicts of interest.

Bibliography

1. Hu, X.; Zou, C.; Zhang, C.; Li, Y. Technological Developments in Batteries: A Survey of Principal Roles, Types, and Management Needs. *IEEE Power and Energy Magazine* **2017**, *15*, 20–31. DOI: 10.1109/MPE.2017.2708812.
2. Tetu, A.; Ferri, F.; Kramer, M.B.; Todalshaug, J.H. Physical and Mathematical Modeling of a Wave Energy Converter Equipped with a Negative Spring Mechanism for Phase Control. *Energies* **2018**, *11*, 2362. DOI: 10.3390/en11092362.
3. Hassan, M.; Balbaa, A.; Issa, H.H.; El-Amary, N.H. Asymptotic Output Tracked Artificial Immunity Controller for Eco–Maximum Power Point Tracking of Wind Turbine Driven by Doubly Fed Induction Generator. *Energies* **2018**, *11*, 2632. DOI: 10.3390/en11102632.
4. Fernendez-Guillamon, A.; Villena-Lapaz, J.; Vigueras-Rodriguez, A.; Garcia-Sanchez, T.; Molina-Garcia, A. An Adaptive Frequency Strategy for Variable Speed Wind Turbines: Application to High Wind Integration into Power Systems. *Energies* **2018**, *11*, 1436. DOI: 10.3390/en11061436.

5. Blanco-M., A.; Gibert, K.; Marti-Puig, P.; Cusido, J.; Sole-Casals, J. Identifying Health Status of Wind Turbines by using Self Organizing Maps and Interpretation–Oriented Post–Processing Tools. *Energies* **2018**, *11*, 723. DOI: 10.3390/en11040723.
6. Bianchi, F.D.; Battista, H.D.; Mantz, R.J. *Wind Turbine Control Systems: Principles, Modelling and Gain Scheduling Design*, 1st ed.; Advances in Industrial Control, Springer, 2007. ISBN: 1–84628–492–9.
7. World Energy Council., Ed. *Cost of Energy Technologies*; World Energy Perspective, World Energy Council: London, UK, 2013. ISBN: 9780946121304. Available at: `www.worldenergy.org`.
8. Odgaard, P.F. FDI/FTC wind turbine benchmark modelling. Workshop on Sustainable Control of Offshore Wind Turbines; Patton, R.J., Ed.; Centre for Adaptive Science & Sustainability, , 2012; Vol. 1.
9. Blanke, M.; Kinnaert, M.; Lunze, J.; Staroswiecki, M. *Diagnosis and Fault–Tolerant Control*; Springer–Verlag: Berlin, Germany, 2006.
10. Odgaard, P.F.; Stoustrup, J.; Kinnaert, M. Fault Tolerant Control of Wind Turbines – a Benchmark Model. Proceedings of the 7th IFAC Symposium on Fault Detection, Supervision and Safety of Technical Processes; , 2009; Vol. 1, pp. 155–160. DOI: 10.3182/20090630–4–ES–2003.0090.
11. Simani, S.; Alvisi, S.; Venturini, M. Study of the Time Response of a Simulated Hydroelectric System. In *Journal of Physics: Conference Series*; Schulte, H.; Georg, S., Eds.; IOP Publishing Limited: Bristol, United Kingdom, 2014; Vol. 570, *Conference Series*, pp. 1–13. ISSN: 1742–6596. DOI: 10.1088/1742-6596/570/5/052003.
12. Zhang, X.; Xu, D.; Liu, Y. Adaptive Optimal Fuzzy Control for Variable Speed Fixed Pitch Wind Turbines. Proceedings of the 5th World Congress on Intelligent Control and Automation, 2004, pp. 2481–2485.
13. Sakamoto, R.; Senjyu, T.; Kinjo, T.; Naomitsu, U.; Funabashi. Output Power Leveling of Wind Turbine Generator by Pitch Angle Control Using Adaptive Control Method. Proceedings of 2004 International Conference on Power System Technology – POWERCON, 2004, pp. 834–839.
14. Johnson, K.E.; Pao, L.Y.; Balas, M.J.; Fingersh, L.J. Control of variable–speed wind turbines: standard and adaptive techniques for maximizing energy capture. *IEEE Control Systems Magazine* **2006**, *26*, 70–81. DOI: 10.1109/MCS.2006.1636311.
15. Zhao, W.; Stol, K. Individual Blade Pitch for Active Yaw Control of a Horizontal–Axis Wind Turbine. Proceedings of the 45th AIAA Aerospace Sciences Meeting and Exhibit; AIAA, AIAA: Reno, NV, USA, 2007.
16. Kishor, N.; Saini, R.; Singh, S. A review on hydropower plant models and control. *Renewable and Sustainable Energy Reviews* **2007**, *11*, 776–796.
17. Hanmandlu, M.; Goyal, H. Proposing a new advanced control technique for micro hydro power plants. *International Journal of Electrical Power & Energy Systems* **2008**, *30*, 272–282.
18. Kishor, N.; Singh, S.; Raghuvanshi, A. Dynamic simulations of hydro turbine and its state estimation based LQ control. *Energy Conversion and Management* **2006**, *47*, 3119–3137.
19. Finotti, S.; Simani, S.; Alvisi, S.; Venturini, M. Benchmarking of Advanced Control Strategies for a Simulated Hydroelectric System. Proc. of the 13th European Workshop on Advanced Control and Diagnosis – ACD2016; Abdel Aitouche, J.K.; Vincent Cocquempot., Eds.; Research Center in Computer Science, Signal and Automatic Control, IOP Publishing. IOP Conf. Series: Lille, France, 2016; Vol. 783, *Journal of Physics: Conf. Series*, pp. 1–12. Invited paper special issue. DOI: 10.1088/1742-6596/783/1/012041.
20. Simani, S.; Ringwood, J.V. Overview of modelling and control strategies for wind turbines and wave energy devices: Comparison and contrasts. *Annual Reviews in Control* **2015**, *40*, 27–49. Special issue invited paper. ISSN: 1367-5788. PII: S1367-5788(15)00037-1 DOI: 10.1016/j.arcontrol.2015.09.003.
21. Simani, S.; Castaldi, P. Active Actuator Fault Tolerant Control of a Wind Turbine Benchmark Model. *International Journal of Robust and Nonlinear Control* **2014**, *24*, 1283–1303. John Wiley. DOI: 10.1002/rnc.2993.
22. Lan, J.; Patton, R.J.; Zhu, X. Fault–tolerant wind turbine pitch control using adaptive sliding mode estimation. *Renewable Energy* **2018**, *116*, 219–231. DOI: 10.1016/j.renene.2016.12.005.
23. Habibi, H.; Nohooji, H.R.; Howard, I. Adaptive PID Control of Wind Turbines for Power Regulation with Unknown Control Direction and Actuator Faults. *IEEE Access* **2018**, *6*, 37464–37479. DOI: 10.1109/ACCESS.2018.2853090.

24. Odgaard, P.F.; Stoustrup, J.; Kinnaert, M. Fault–Tolerant Control of Wind Turbines: A Benchmark Model. *IEEE Transactions on Control Systems Technology* **2013**, *21*, 1168–1182. ISSN: 1063–6536. DOI: 10.1109/TCST.2013.2259235.
25. David Rivkin, D.; Anderson, L.D.; Silk, L. *Wind Turbine Control Systems*, 1st ed.; Jones & Bartlett Learning, 2012. ISBN: 978–1449624538.
26. de Mello, F.P.; Koessler, R.J.; Agee, J.; Anderson, P.M.; Doudna, J.H.; Fish, J.H.; Hamm, P.A.L.; Kundur, P.; Lee, D.C.; Rogers, J.; Taylor, C. Hydraulic turbine and turbine control models for system dynamic studies. *IEEE Transactions on Power Systems* **1992**, *7*, 167–179. DOI:.
27. Venturini, M.; Alvisi, S.; Simani, S.; Manservigi, L. Development of a physics–based model to predict the performance of pumps as turbines (PATs). Proc. of ECOS2017 – the 30th International Conference on Efficiency, Cost, Optimization, Simulation and Environmental Impact of Energy Systems; San Diego State University, `https://ecos2015.sciencesconf.org`: San Diego, California, USA, 2017; pp. 1–16. (Invited Paper).
28. Popescu, M.; Arsenie, D.; Vlase, P. *Applied Hydraulic Transients: For Hydropower Plants and Pumping Stations*; CRC Press: Lisse, The Netherlands, 2003.
29. Simani, S.; Alvisi, S.; Venturini, M. Fault Tolerant Control of a Simulated Hydroelectric System. *Control Engineering Practice* **2016**, *51*, 13–25. DOI: http://dx.doi.org/10.1016/j.conengprac.2016.03.010.
30. Fang, H.; Chen, L.; Dlakavu, N.; Shen, Z. Basic Modeling and Simulation Tool for Analysis of Hydraulic Transients in Hydroelectric Power Plants. *IEEE Trans. Energy Convers.* **2008**, *23*, 424–434.
31. Chaudhry, M.H. *Applied Hydraulic Transients*, 3rd ed.; Springer, 2013. ISBN: 9781461485377.
32. Vournas, C.D.; Papaionnou, G. Modeling and stability of a hydro plant with two surge tanks. *IEEE Trans. Energy Convers.*Jun., *10*, 368–375.
33. Urquiza Beltrán, G.; Castro Gómez, L.L., Eds. *Flow Measurement*; Control Engineering, InTech, 2012. DOI: 10.5772/2111. ISBN: 9789535103905.
34. Simani, S.; Farsoni, S. *Fault Diagnosis and Sustainable Control of Wind Turbines: Robust data–driven and model–based strategies*, 1st ed.; Mechanical Engineering, Butterworth–Heinemann – Elsevier: Oxford (UK), 2018. ISBN: 9780128129845.
35. Slotine, J.E.; Li, W. *Applied Nonlinear Control*; Prentice-Hall, 1991.
36. Åström, K.J.; Hägglund, T. *Advanced PID Control*; ISA - The Instrumentation, Systems, and Automation Society: Research Triangle Park, NC 27709, 2006. ISBN: 978–1–55617–942–6.
37. Jang, J.S.R. ANFIS: Adaptive–Network–based Fuzzy Inference System. *IEEE Transactions on Systems, Man., & Cybernetics* **1993**, *23*, 665–684.
38. Jang, J.S.R.; Sun, C.T. *Neuro–Fuzzy and Soft Computing: A Computational Approach to Learning and Machine Intelligence*, 1st ed.; Prentice Hall, 1997. ISBN: 9780132610667.
39. Babuška, R. *Fuzzy Modeling for Control*; Kluwer Academic Publishers: Boston, USA, 1998.
40. Bobál, V.; Böhm, J.; Fessl, J.; Machácek, J. *Digital Self–Tuning Controllers: Algorithms, Implementation and Applications*, 1st ed.; Advanced Textbooks in Control and Signal Processing, Springer, 2005.
41. Simani, S.; Alvisi, S.; Venturini, M. Fault Tolerant Model Predictive Control Applied to a Simulated Hydroelectric System. Proceedings of the 3rd International Conference on Control and Fault–Tolerant Systems – SysTol'16; Control Systems Society, I., Ed.; Research Center for Supervision, Safety and Automatic Control of the Universitat Politècnica de Catalunya in Barcelona, IEEE: Barcelona, Spain, 2016; pp. 251–256. ISBN: 978–5090–0657–1. ISSN: 2162-1209. DOI: 10.1109/SYSTOL.2016.7739759. Special session invited paper.
42. Odgaard, P.F.; Stoustrup, J. Unknown Input Observer Based Scheme for Detecting Faults in a Wind Turbine Converter. Proceedings of the 7th IFAC Symposium on Fault Detection, Supervision and Safety of Technical Processes; IFAC – Elsevier: Barcelona, Spain, 2009; Vol. 1, pp. 161–166. DOI: 10.3182/20090630–4–ES–2003.0048.
43. Brown, M.; Harris, C. *Neurofuzzy Adaptive Modelling and Control*; Prentice Hall, 1994.
44. Mahmoud, M.; Dutton, K.; Denman, M. Design and simulation of a nonlinear fuzzy controller for a hydropower plant. *Electric Power Systems Research* **2005**, *73*, 87–99.

 doi:10.20944/preprints201810.0572.v1